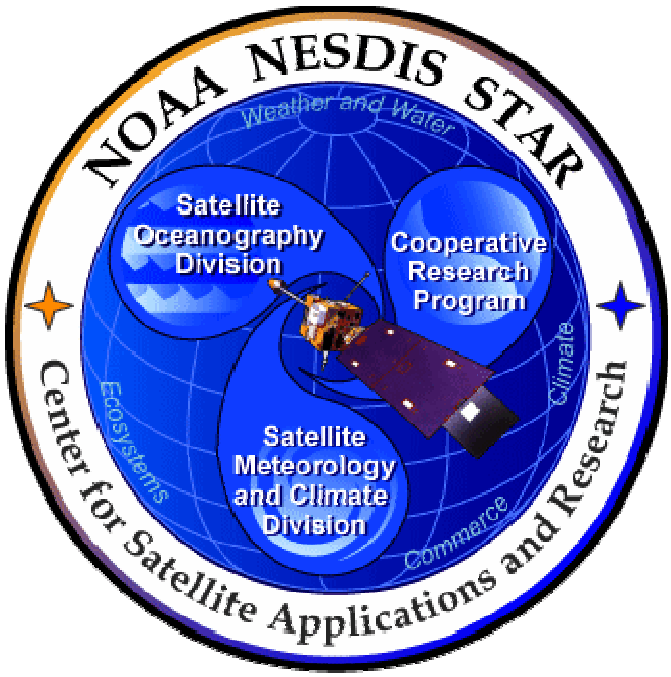

NOAA NESDIS
CENTER for SATELLITE APPLICATIONS and RESEARCH

ALGORITHM THEORETICAL BASIS DOCUMENT

ABI Ice Thickness and Age

Xuanji Wang, UW/CIMSS

Jeffrey R. Key, NOAA/NESDIS/STAR

Version 1.1, 80%

September 15, 2010

TABLE OF CONTENTS

LIST OF FIGURES

LIST OF TABLES

LIST OF ACRONYMS

ABI - Advanced Baseline Imager
AIT - Algorithm Integration Team
AITA - ABI Ice Thickness and Age
APP-x – Extended AVHRR Polar Pathfinder
ATBD - algorithm theoretical basis document
AVHRR - Advanced Very High Resolution Radiometer
AWG - Algorithm Working Group
CIMSS - Cooperative Institute for Meteorological Satellite Studies
CIS - Canadian Ice Service
CSIM - CSM Sea Ice Model
CSM – Climate System Model
ECMWF - European Centre for Medium-Range Weather Forecasts
F&PS - Function and Performance Specification
GCM – Global Circulation Model
GOCC - Generalized Orthogonal Curvilinear Coordinate
GOES - Geostationary Operational Environmental Satellite
MODIS - Moderate Resolution Imaging Spectroradiometer
MRD - Mission Requirements Document
MSG - Meteosat Second Generation
NASA - National Aeronautics and Space Administration
NCAR - National Center for Atmospheric Research
NCEP - National Centers for Environmental Prediction
NOAA - National Oceanic and Atmospheric Administration
NSIDC - National Snow and Ice Data Center
NWP - Numerical Weather Prediction
OTIM - One-dimensional Thermodynamic Ice Model
PIOMAS - Pan-Arctic Ice-Ocean Modeling and Assimilation System
POP - Parallel Ocean Program
RTM - Radiative Transfer Model
SCICEX - SCientific ICe EXpeditions
SEVIRI - Spinning Enhanced Visible and Infrared Imager
SHEBA - Surface HEat Balance of the Arctic Ocean
SIT – Sea Ice Temperature
SIC – Sea Ice Concentration
SSEC – Space Science and Engineering Center
TED - Thickness and Enthalpy Distribution
TOA – Top of Atmosphere
ULS – Upward Looking Sonar
UW – University of Wisconsin

ABSTRACT

This document provides a high level description of the physical basis for determining sea and lake ice thickness and age information of each clear pixel within images taken by the Advanced Baseline Imager (ABI) flown on the GOES-R series of NOAA geostationary meteorological satellites. As ice age is determined from the ice thickness information within the same algorithm module, both are described in this ATBD.

The core of the ABI ice thickness and age algorithm is a One-dimensional Thermodynamic Ice Model (OTIM). Based on the surface energy budget at thermo-equilibrium, OTIM contains all the components of the surface energy budget that are needed for estimating sea and lake ice thickness. Based on its thickness, ice is classified as open water, new/fresh ice, grey ice, grey-white ice, thin first year ice, medium first year ice, thick first year ice, or multi-year or old ice. As needed, the OTIM contains parameterizations and/or assumptions of the sea and lake ice and associated snow characteristics of their physical properties, such as ice and snow conductivities, densities, and transmittances, if that information is not available. The validation analysis indicates that the algorithm can meet the accuracy requirements of the Functional and Performance Specification (F&PS).

1 INTRODUCTION

1.1 Purpose of This Document

This algorithm theoretical basis document (ATBD) provides a high level description of the physical basis for the estimating ice thickness and age for clear and cloudy pixels identified as ice covered using supplementary information from parameterization schemes and other products retrieved from the Advanced Baseline Imager (ABI) flown on the GOES-R series of NOAA geostationary meteorological satellites. That supplementary information includes a cloud mask, snow depth, ice surface temperature, ice concentration, surface air temperature, surface air humidity, surface wind, and surface solar and thermal radiation fluxes. The ice thickness and age algorithm provides primary estimates of the ice thickness and age for each ABI pixel covered with ice. The ice thickness and age products are made available to all subsequent algorithms that require knowledge of ice information.

1.2 Who Should Use This Document

The intended users of this document are those interested in understanding the physical basis of the algorithm and how to use the output of this algorithm to estimate ice thickness and age for a particular application. This document also provides information useful to anyone maintaining or modifying the original algorithm.

1.3 Inside Each Section

This document is broken down into the following main sections.

- **System Overview**: Provides relevant details of the ABI and a brief description of the products generated by this algorithm.

- **Algorithm Description**: Provides a detailed description of the algorithm including its physical basis, its input and its output.

- **Assumptions and Limitations**: Provides an overview of the current limitations of the approach and notes the plan for overcoming these limitations with further algorithm development.

1.4 Related Documents

This document currently does not relate to any other document outside of the specifications of the GOES-R Mission Requirements Document (MRD) and to the references given through out.

1.5 Revision History

Version 1.0 of this document was modified and updated by Xuanji Wang of UW/CIMSS and Jeff Key of NOAA/NESDIS/STAR based on the previous versions of this document, and is intended to accompany the delivery of the version 3.0 algorithms to the GOES-R AWG Algorithm Integration Team (AIT).

Version 0.0 of this document was created by Xuanji Wang of UW/CIMSS and Jeff Key of NOAA/NESDIS/STAR, and was intended to accompany the delivery of the version 0.0 algorithms to the GOES-R AWG Algorithm Integration Team (AIT).

2 OBSERVING SYSTEM OVERVIEW

This section describes the products generated by the ABI Ice Thickness and Age (AITA) algorithm and the requirements it places on the sensor and other products.

2.1 Products Generated

The ice thickness and age algorithm is responsible for estimating sea and lake ice thickness and age for all ABI pixels covered with ice. Following the Threshold level of the GOES-R MRD, ice-free areas are distinguished from first-year ice and older ice areas. The Goal requirement of the MRD is to distinguish not only ice-free from first-year ice areas, but also to distinguish between the following types of ice based on age: nilas, grey white, first-year thin, first-year medium, first-year thick, second-year, multiyear smooth and multiyear deformed ice. The ice thickness and age products will be used by other ABI algorithms that require knowledge of ice information. The current ice thickness and age design has the ability to estimate sea and lake ice thickness up to 3 meters under both clear and cloudy conditions at night (no sunlight). While it would also work during daytime, the estimation is more uncertain due to the complexities of ice and snow optical properties in the solar spectrum. The required products Function and Performance Specification (F&PS) is listed in Table 1 below. Details on determining ice age are described in Sections 3.1 and 3.4.2.9.

Table 1. Products Function and Performance Specification (F&PS).

Name	User & Priority	Geographic Coverage (G, H, C, M)	Vertical Resolution	Horizontal Resolution	Mapping Accuracy	Measurement Range	Measurement Accuracy	Product Refresh Rate/Coverage	Vendor Allocated Ground Latency	Product Measurement Precision
Sea & Lake Ice: Age	GOES-R	FD	Ice Surface	1 km	3 km	Ice free areas, First year ice Older Ice	80% correct classification	6 hr	3236 sec	1 category

Name	User & Priority	Geographic Coverage (G, H, C)	Temporal Coverage Qualifiers	Product Extent Qualifier	Cloud Cover Conditions Qualifier	Product Statistics Qualifier
Sea & Lake Ice: Age	GOES-R	FD	Sun at less than 67 degree solar zenith angle	Quantitative out to at least 67 degrees LZA and qualitative at larger LZA	Clear conditions associated with threshold accuracy	Over specified geographic area

2.2 Instrument Characteristics

The ice thickness and age will be produced for each pixel observed by the ABI and covered with ice. While there are no direct ABI channels related to the algorithm, it relies on other retrieved products from ABI and parameterization schemes such as cloud mask, ice surface temperature, ice surface albedo, and radiation fluxes that would use some or all ABI channels for their retrievals. As a result, the performance of the ice thickness and age algorithm is sensitive to the accuracy of other ABI retrieved products. We will detail the required input parameters and current validations in the following sections, as well as the algorithm sensitivity to input uncertainties.

Table 2. Summary of the Current ABI Channel Numbers and Wavelengths.

Channel Number	***Wavelength (μm)***	***Direct Use in AITA***
1	0.47	No
2	0.64	No
3	0.86	No
4	1.38	No
5	1.61	No
6	2.26	No
7	3.9	No
8	6.15	No
9	7.0	No
10	7.4	No
11	8.5	No
12	9.7	No
13	10.35	No
14	11.2	No
15	12.3	No
16	13.3	No

3 ALGORITHM DESCRIPTION

This section contains a complete description of the algorithm at its current level of maturity (which will improve with each revision).

3.1 Algorithm Overview

The ice thickness and age algorithm will use a One-dimensional Thermodynamic Ice Model (OTIM) developed by the investigators. OTIM is based on the surface energy balance at thermo-equilibrium and contains all the components of the surface energy budget to estimate sea and lake ice thickness up to 3 meters. Ice age is based on ice thickness as follows:

- Free or Open water: thickness = 0
- New: 0.00 < thickness ≤ 0.10
- Grey: 0.10 < thickness ≤ 0.15
- Grey-white: 0.15 < thickness ≤ 0.30
- First year Thin: 0.30 < thickness ≤ 0.70
- First year Medium: 0.70 < thickness ≤ 1.20
- First year Thick: 1.20 < thickness < 1.80
- Older: thickness ≥ 1.80

Pros:

- Solid physical foundation with all components of the surface energy budget considered.
- Capable of retrieving daytime and nighttime sea and lake ice thickness under both clear and cloudy sky conditions.
- Very computationally efficient compared to more complex models such as the Climate System Model (CSM) Sea Ice Model (CSIM).
- Its sole objective of retrieving ice thickness and age makes it easy to implement with the application of satellite products, flexible, fast and easy to maintain and improve later with more and accurate satellite derived products like radiative fluxes, ice surface temperature and snow depth over the ice.

Cons:

- The accuracy of input parameters, e.g., snow depth, surface air humidity, temperature, and wind, will impact the accuracy of ice thickness estimates.
- Daytime retrieval is sensitive to ice optical properties associated with ice type and thickness, and is less reliable than nighttime retrievals.

3.2 Processing Outline

The processing outline of the AITA is summarized in the following chart. The AITA is designed to run on segments of data. A segment is comprised of multiple scan lines.

High Level Flowchart of the AITA Illustrating the Main Processing Sections.

.

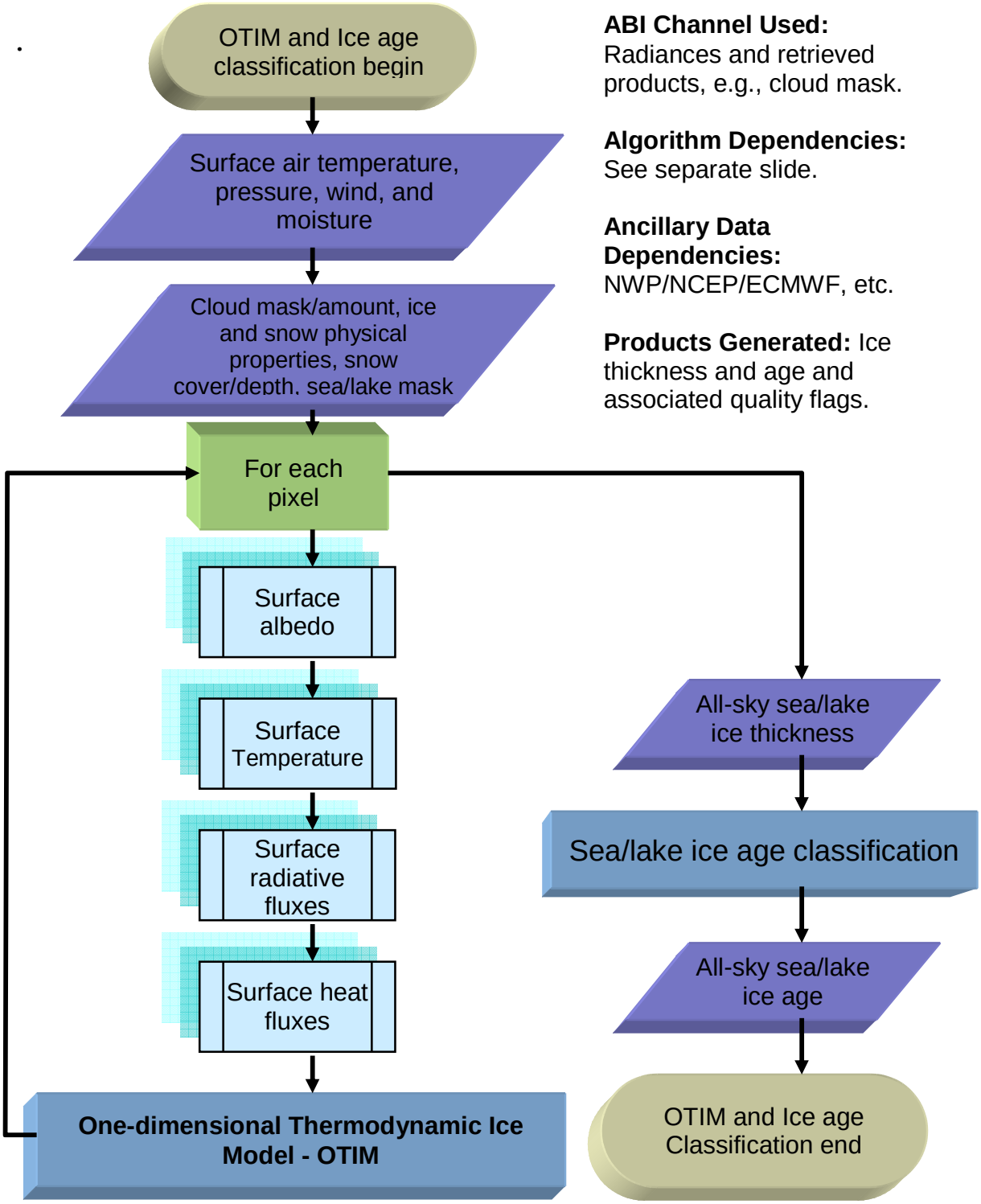

ABI Channel Used: Radiances and retrieved products, e.g., cloud mask.

Algorithm Dependencies: See separate slide.

Ancillary Data Dependencies: NWP/NCEP/ECMWF, etc.

Products Generated: Ice thickness and age and associated quality flags.

The AITA Algorithm Dependency on Other ABI Products and Data Sources.

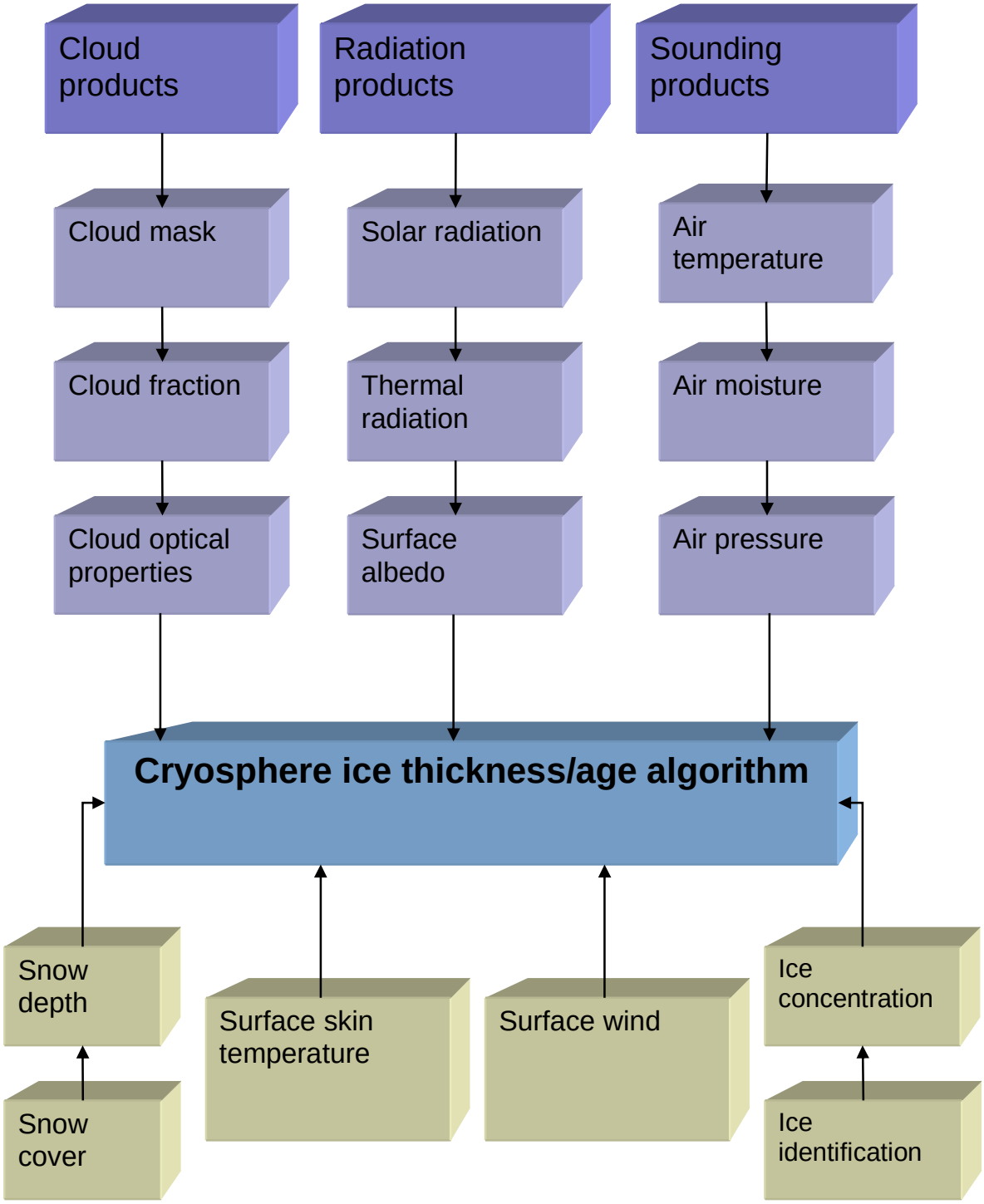

3.3 Algorithm Input

This section describes the input needed to process the AITA. While the AITA is derived for each pixel covered with ice, it does require knowledge of the surrounding atmosphere. In this version, the daytime retrieval was run and improved, but it will still be investigated in the next version due to the fact that complex solar radiation interactions result in a larger uncertainty than with nighttime applications.

3.3.1 Primary Sensor Data

The list below contains the primary data used by the AITA, information that is derived mainly from the ABI observations and geolocation information.

- **Sensor viewing zenith angle**
- **Solar zenith angle**
- **Relative azimuth angle**
- **Glint zenith angle**
- **Scattering angle**

3.3.2 Ancillary Data

The following list briefly describes the ancillary data required to run the AITA, information that is not included in the ABI observations or geolocation data. Land/coast masks can be obtained from the U.S. Geological Survey (USGS) and/or some software packages like IDL, while ice and snow properties can be collected by many experiments and measurements published in the literature. Surface air temperature/humidity/pressure/wind can be acquired from numerical model forecasts such as the NOAA Global Forecast System (GFS) and/or European Centre for Medium-Range Weather Forecasts (ECMWF), to be used for the bulk transfer calculations for turbulent heat fluxes (see Sections 3.4.2.5 and 3.4.2.6 for details).

- **Land mask**
- **Coast mask**
- **Ice and Snow Thermal Emissivity**
- **Ice and Snow Optical Properties (Albedo, Transmittance, Absorptivity)**
- **Ice and Snow Physical Properties (Density, Salinity, Conductivity, Contaminant)**
- **Surface Air Temperature**
- **Surface Humidity**
- **Surface Wind**

3.3.3 Derived Data

The following briefly describes the products from other ABI algorithms that the AITA algorithm uses as input. These data are necessary in order to run the software that calculates ice thickness and sequentially ice age. These data are required information that is not included in the ABI observations or geo-location data.

- **surface broadband albedo**
- **cloud mask and cloud fraction**
- **ice/snow surface skin temperature**
- **ice mask and concentration**
- **snow mask and snow depth**

3.4 Theoretical Description

Physical and/or statistical approaches are employed to estimate sea and lake ice thickness and age. In this document, a One-dimensional Thermodynamic Ice Model (OTIM) based on the surface energy budget at thermo-equilibrium, containing all components of the surface energy budget, has been developed to estimate sea and lake ice thickness. Based on knowledge of the ice thickness, ice is classified as open water, new/fresh ice, grey ice, grey-white ice, thin first year ice, medium first year ice, thick first year ice, or multi-year or older ice. Categorizing the ice thickness inevitably involves parameterizations and/or assumptions of the sea and lake ice and associated snow characteristics, such as ice and snow conductivities, densities, and transmittances.

3.4.1 Physics of the Problem

Any ice thickness and age estimation based on thermodynamic theory is complicated by the need to exploit not only ice and snow micro-physical properties which are closely related to ice and snow types and contents but also environmental conditions such as humidity, air temperature, wind, cloud cover, water salinity and current. In the testing stage of the AITA, we have extensively used information from:

- the extended AVHRR Polar Pathfinder (APP-x) product, which consists of AVHRR retrievals of surface and cloud properties using our retrieval tool CASPR (Key, 2002) for the period 1982-2004 over the Arctic;
- the NCAR/NCEP Reanalysis data;
- parameterization schemes for ice and snow micro-physical properties;
- solar and thermal radiation flux parameterizations at the surface developed by other researchers; as well as
- MODIS and SEVIRI data.

While the current NCAR/NCEP Reanalysis fields often have errors in some critical fields, such as the surface air temperature and humidity over ice and snow, they provide needed and useful information. Nevertheless, parameterization schemes are often required to estimate environmental conditions, especially for ice and snow areas.

The AITA uses the OTIM to estimate sea and lake ice thickness. The OTIM treats day and night retrievals differently. When the sun is above the horizon, the solar radiation must be considered in the OTIM which complicates the ice thickness estimation; the inability to correctly identify the ice and snow types results in inaccurate ice and snow optical property estimates in the solar spectrum, as well as unstable numerical solutions for the OTIM. Nighttime retrievals of ice thickness are easier and more accurate, with an analytical solution in the OTIM. The OTIM has been tested with AVHRR, MODIS, and SEVIRI data and validated with submarine and moored Upward Looking Sonar data, meteorological station measurements, and numerical model simulations.

3.4.2 Mathematical Description

A slab model proposed by Maykut and Untersteiner (1971) is used here as a prototype model. The equation for energy conservation at the top surface (ice or snow) is

$$(1-\alpha_s)F_r - I_0 - F_l^{up} + F_l^{dn} + F_s + F_e + F_c = F_a$$

or

$$(1-\alpha_s)(1-i_0)F_r - F_l^{up} + F_l^{dn} + F_s + F_e + F_c = F_a \qquad (1)$$

where α_s is the ice surface broadband albedo where ice may be covered with a layer of snow, F_r is the downward solar radiation flux at the surface, I_0 is the solar radiation flux passing through the ice interior and i_0 is the ice slab transmittance, F_l^{up} is the upward longwave radiation flux from the surface, F_l^{dn} is the downward longwave radiation flux from the atmosphere towards the surface, F_s is the turbulent sensible heat flux at the surface, F_e is the turbulent latent heat flux at the surface, F_c is the conductive heat flux within the ice slab, F_a is the residual heat flux that could be caused by ice melting and/or heat advection. By the definitions of the terms in the equation (1), α_s, F_r, I_0, F_l^{up}, F_l^{dn} should be always positive, and F_s, F_e, and F_c would be positive or negative in terms of the operational symbols used in equation (1), and F_a is zero in the absence of a phase change or horizontal heat flux exchange. The details of each term will be addressed in the following subsections.

3.4.2.1 Solar Radiation at the Surface

The first term on the left-hand side of the equation (1), $(1-\alpha_s)F_r$, is the net solar radiation flux at the surface. The surface broadband albedo over entire solar spectrum, α_s, can be input or estimated by the Thomas C. Grenfell (1979) method as described below:

$$\alpha_s = 1 - A\exp(-Bh) - C\exp(-Dh) \qquad (2)$$

where ***A, B, C***, and ***D*** are the coefficients the values of which can be determined from Table 3 below, and ***h*** is the ice (h_i) or snow (h_s) thickness in meters. The other relatively simple approach to determine ice and snow surface albedo includes model simulated constant values based on the ice and snow types as discussed by Tuomo M. Saloranta (2000), and the experimental and observational values for a variety of snow and ice surface conditions (Grenfell and Perovich, 2004) as shown in Figure 1 from Donald K. Perovich (1996).

Table 3. The coefficient values of A, B, C, and D in Eq. (2) (from Thomas C. Grenfell, 1979)

Ice type	***Cloudiness***	***A***	***B***	***C***	***D***	***Error***
Blue ice 0.8m >= h_i>=0.02m	Clear	0.130	15.46	0.820	0.1216	< 1%
	Cloudy	0.150	12.02	0.800	0.2161	< 1%
White ice 0.8m >= h_i>=0.02m	Clear	0.419	12.40	0.531	0.1958	< 2.5%
	Cloudy	0.540	10.11	0.410	0.2827	< 3%
Dry packed snow over blue ice 0.4m >= h_s >= 0.01m	Clear	0.2213	77.48	0.1980	0	< 5%
	Cloudy	0.3181	77.81	0.100	0.050	< 7%

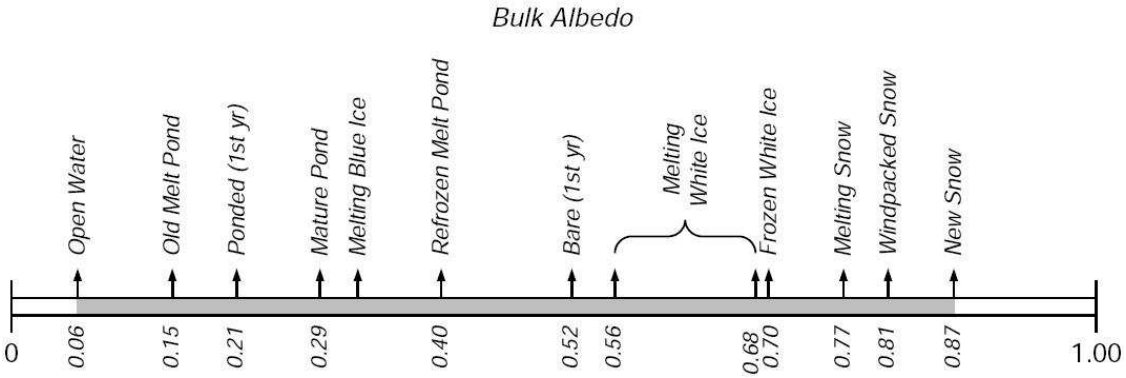

Figure 1. Range of observed values of total albedo for sea ice. The albedos are from Burt (1954), Chernigovskiy (1963), Langleben (1971), Grenfell and Maykut (1977), and Grenfell and Perovich (1984).

The downward shortwave radiation flux towards the surface, F_r, could also be an input parameter for the OTIM or parameterized with model built-in parameterization schemes under both clear and cloudy sky conditions as described below. Key (1996) compared these schemes and discussed which scheme would be better regarding the surface type, location, and atmospheric conditions.

3.4.2.1.1 Clear-sky Parameterizations of Solar Radiation

1. Shine and Henderson-Sellers (1985) scheme for the Arctic:

$$F_r^{clr} = 1368\mu^2[1.2\mu + (1.0 + \mu)\, e_a\, 10^{-3} + 0.046]^{-1} \qquad (3)$$

where μ is the cosine of the solar zenith angle, $e_a = f \cdot e_{sa}$, e_a is the surface water vapor pressure (*hPa*), e_{sa} is the surface saturation water vapor pressure (*hPa*), and f is relative humidity (%). Knowing the surface air temperature T_a (C) and relative humidity f, we can calculate e_a by

$$e_{sa} = 6.11*10.0\text{^}(7.5*T_a / (237.7 + T_a)) \qquad (4)$$

where $e_a = f\, e_{sa}$.

2. Moritz (1978) scheme for Baffin Bay, Canada:

$$F_r^{clr} = S_0\, \mu\, (0.47 + 0.47\, \mu) \qquad (5)$$

where S_0 is the solar constant, and μ is the cosine of the solar zenith angle.

3. Bennett (1982) scheme for the Arctic:

$$F_r^{clr} = 0.72\, S_0\, \mu \qquad (6)$$

where S_0 and μ are the same as above. This scheme is recommended for its simplicity and acceptable accuracy.

3.4.2.1.2 Cloudy-sky Parameterizations of Solar Radiation

1. Berliand (1960) scheme:

$$F_r^{all} = F_r^{clr}\, (1 - x\, c - y\, c^2) \qquad (7)$$

where c is the cloud fraction between 0~1. For land and ocean, *y=0.38*, *x=0.14* at 85^o, *0.41* at 55^o, and *0.38* at 45^o respectively; and *x=0.45* and *y=0* at 75^oN or 75^oS. Its performance has tested poor over oceans.

2. Laevastu (1960) scheme for the mid-latitude ocean:

$$F_r^{all} = F_r^{clr}\, (1 - 0.6\, c^3) \qquad (8)$$

3. Jacobs (1978) scheme for Baffin Island, Canada over the period June to October:

$$F_r^{all} = F_r^{clr}\, (1 - 0.33\, c) \qquad (9)$$

4. Bennett (1982) scheme for Arctic sea ice:

$$F_r^{all} = F_r^{clr} (1 - 0.52\, c) \qquad (10)$$

This scheme is recommended for its simplicity and acceptable accuracy for this study.

5. Shine (1984) scheme for high albedo surfaces such as ice and snow:

$$F_r^{cld} = (53.5 + 1274.5\, \mu)\, \mu^{0.5} / [1 + 0.139\, (1 - 0.9345\, \alpha_s)\, \tau] \qquad (11)$$

$$F_r^{all} = [(1 - c)\, F_r^{clr} + c\, F_r^{cld}] \qquad (12)$$

where α_s is the surface broadband albedo (0~1), and τ is the cloud optical depth.

3.4.2.2 Solar Radiation Passing through Ice Interior

The second term on the left-hand side of the equation (1), $I_0 = i_0\, (1-\alpha_s) F_r$, is the solar radiation flux passing through the ice interior. i_o is the ice slab transmittance, i.e., the percentage of the net solar radiation flux that penetrates the ice, which can be estimated by the following parameterization scheme developed by Thomas G. Grenfell (1979):

$$i_0 = A\, exp(-Bh) + C\, exp(-Dh) \qquad (13)$$

where ***A, B, C***, and ***D*** are the coefficients given in Table 4, and *h* is the ice slab thickness in meters.

Table 4. The coefficient values of A, B, C, and D in Eq. (13) (from Thomas C. Grenfell, 1979)

Ice Type	*Cloudiness*	*A*	*B*	*C*	*D*	*Error*
Blue ice 0.8m >= h_i >=0.02m	Clear Cloudy	0.1925 0.1553	12.96 12.84	0.515 0.755	1.227 1.081	< 4% < 2%
White ice 0.8m >= h_i >= 0.02m	Clear Cloudy	0.3894 0.3456	12.39 10.30	0.350 0.590	1.578 1.315	< 4% < 2.5%
Dry packed snow over blue ice 0.4m >= h_s >= 0.01m 0.8m >= h_i >= 0.01m	Clear	$A = 0.2257 \exp(-16.73h_s) + 0.4174 \exp(-43.89h_s)$ $B = 0.7280 \exp(-0.1862\, h_s) + 0.3532 \exp(-13.04h_s)$ $C = 0.1561 \exp(-92.79h_s)$ $D = [0.06 + 0.0995 \exp(-94.20h_s)]^{-1}$				
	Cloudy	< 6% $A = 0.980 \exp(-17.81h_s)$ $B = 0.6945 \exp(-0.1048h_s) + 0.303 \exp(-54.92h_s^{1.42})$ $C = D = 0.0$				
		< 6%				

In the first approximation, the parameter i_o for the percentage of shortwave radiation penetrating into snow is kept at zero, and i_o for ice is calculated linearly as a function of cloudiness as given in Grenfell and Maykut's 1977 paper:

$i_o = 0.18(1-c) + 0.35c$ for white ice thickness less than 0.1 m,

$i_o = 0.43\ (1-c) + 0.63c$ for blue ice thickness less than 0.1 m,

where c is cloud fraction.

3.4.2.3 Upward Longwave Radiation from the Surface

The third term on the left-hand side of the equation (1), F_l^{up}, is the upward longwave radiation flux from the surface that can be easily estimated with the following formula:

$$F_l^{up} = \varepsilon\ \sigma\ T_s^4 \qquad (14)$$

where ε is the longwave emissivity of the ice or snow surface, $\sigma = 5.6696*10^{-8}\ W\ m^{-2}\ deg^{-4}$ is the Stefan-Boltzman constant, and T_s is the surface skin temperature in K. For simplicity, an emissivity of *0.988* is used for ice. Even though some pixels contain a small portion of open water or snow surface, the emissivity error from incorrectly specifying the surface type is small because the snow emissivity at a 0^o look angle is *0.995*, very close to the value of *0.987* for ice and *0.988* for water (Rees, 1993).

3.4.2.4 Downward Longwave Radiation towards the Surface

The fourth term on the left-hand side of the equation (1), F_l^{dn}, is the downward longwave radiation flux from the atmosphere towards the surface that can be parameterized by the following schemes.

3.4.2.4.1 Clear-sky Parameterizations of Longwave Radiation

1. Yu and Rothrock (1996) scheme:

$$F_l^{dn} = \varepsilon^*\ \sigma\ T_a^4 \qquad (15)$$

where $\varepsilon^* = 0.7855\ (1 + 0.2232\ c^{2.75})$ is an effective emissivity for the atmosphere and T_a is the near-surface air temperature at *2* m above the surface, and c is the fractional cloud cover.

2. Efimova (1961) scheme:

$$F_{l,clr}^{dn} = \sigma\ T_a^4\ (0.746 + 0.0066\ e_a) \qquad (16)$$

where e_a is the water vapor pressure (*hPa*).

3. Ohmura (1981) scheme for the temperature range *243-289K*:

$$F_{l,clr}^{dn} = \sigma T_a^4 (8.733*10^{-3} T_a^{0.788}) \quad (17)$$

where σ, and T_a are the same as above. This scheme is recommended for its simplicity and acceptable accuracy for this work.

4. Maykut and Church (1973) scheme for the temperature range *244-277K*:

$$F_{l,clr}^{dn} = 0.7855 \sigma T_a^4 \quad (18)$$

where σ, and T_a are the same as above.

5. Andreas and Ackley (1982) scheme for the Arctic and Antarctic regions:

$$F_{l,clr}^{dn} = \sigma T_a^4 (0.601 + 5.95*10^{-5} e_a^{1500/Ta}) \quad (19)$$

where σ, and T_a are the same as above, and e_a is the near-surface water vapor pressure (*hPa*).

3.4.2.4.2 Cloudy-sky Parameterizations of Longwave Radiation

1. Yu and Rothrock (1996) scheme:

$$F_l^{dn} = \varepsilon^* \sigma T_a^4 \quad (20)$$

where $\varepsilon^* = 0.7855 (1 + 0.2232 c^{2.75})$ is an effective emissivity for the atmosphere and T_a is the near-surface air temperature at 2 m above the surface, and c is the fractional cloud cover.

2. Jacobs (1978) scheme for Arctic summer and winter:

$$F_l^{dn} = F_{l,clr}^{dn} (1 + 0.26 c) \quad (21)$$

where c is the fractional cloud cover. This scheme is recommended for the simplicity and acceptable accuracy for this work.

3. Maykut and Church (1973) scheme over *244-277K*:

$$F_l^{dn} = F_{l,clr}^{dn} (1 + 0.22 c^{2.75}) \quad (22)$$

where c is the fractional cloud cover.

4. Zillman (1972) scheme:

$$F_l^{dn} = F_{l,clr}^{dn} + \sigma T_a^4 0.96 (1 - 9.2*10^{-6} T_a^2) c \quad (23)$$

5. Schmetz et al. (1986) scheme:

$$F_l^{dn} = F_{l,clr}^{dn} + (1 - \varepsilon_0)\, C\, \varepsilon_c\, \sigma\, T_0^4\, exp[(T_B + T_0) / 46] \qquad (24)$$

where ε_0 is the effective sky emittance, ε_c is the cloud emissivity, T_0 is the near-surface air temperature, and T_B is the cloud base temperature.

3.4.2.5 Turbulent Sensible Heat Flux

The fifth term on the left-hand side of the equation (1), F_s, is the turbulent sensible heat flux at the surface that can be calculated by the following formulae if it is an unknown variable in the OTIM.

$$F_s = \rho_a\, c_p\, C_s\, u\, (T_a - T_s) \qquad (25)$$

where ρ_a is the air density (standard value of *1.275* kg·m^{-3} at 0^{o}C and 1000 hPa), c_p is the specific heat of wet air that should be calculated from Eq. (25.1) with wet air specific humidity q, C_s is the bulk transfer coefficients for the turbulent sensible heat flux between the air and ice surface (Yu chose C_s = *0.003* for very thin ice, and *0.00175* for thick ice, *0.0023* for neutral stratification as suggested by Lindsay (1998) in his energy balance model for thick arctic pack ice), u is the surface wind speed, T_a is the near surface air temperature at *2* m above the surface, and T_s is the surface skin temperature.

$$C_p = C_{pd}(1 - q + \frac{C_{pv}}{C_{pd}} q) \qquad (25.1)$$

where C_{pv} is the specific heat of water vapor at constant pressure (1952 J K^{-1} kg^{-1}), and C_{pd} is the specific heat of dry air at constant pressure (1004.5 J K^{-1} kg^{-1}), so C_p can simply be written as C_p=1004.5·(1+0.9433·q).

The wet air density ρ_a can be calculated using the gas law with a given surface air pressure P_a (hPa), surface air virtual temperature T_v (K), and gas constant R_{gas} (287.1 J kg^{-1} K^{-1}) by Eq. 25.2.

$$\rho_a = \frac{100 P_a}{R_{gas} T_v} \qquad (25.2)$$

where T_v=(1 + 0.608·q)·T_a, q is the wet air specific humidity (kg/kg).

3.4.2.6 Turbulent Latent Heat Flux

The sixth term on the left-hand side of the equation (1), F_e, is the turbulent latent heat flux at the surface that can be calculated by the following formulae if it is an unknown variable in the OTIM.

$$F_e = \rho_a\, L\, C_e\, u\, (w_a - w_{sa}) \qquad (26)$$

where ρ_a is the air density, L is the latent heat of vaporization ($2.5 \cdot 10^6$ J·kg^{-1}) which should include the latent heat fusion/melting ($3.34 \cdot 10^5$ J·kg^{-1}) if the surface is below freezing, C_e is the bulk transfer coefficients for latent heat flux of evaporation, u is surface wind speed, w_a is the air mixing ratio at 2 m, w_{sa} is the mixing ratio at the surface. The mixing ratio is very close to the specific humidity in magnitude, $w = q/(1-q) \cong q$, where q is the specific humidity.

The bulk transfer coefficient C_e for the latent heat flux is a function of wind speed and air-sea ice temperature difference which can be parameterized as described by Bentamy et al (2003),

$$C_e = \{ a \exp[b (u + c)] + d/u + 1 \} x 10^{-3}, \qquad (26.1)$$

where a=-0.146785, b=-0.292400, c=-2.206648, and d=1.6112292. The C_e values range between 0.0015 and 0.0011 for wind speeds between 2 and 20 m s^{-1}. Schroder et al's study (2003) indicated that C_e values are always around 1.0x10^{-3} except for rough multi-year ice which has a C_e value of 1.3x10^{-3}, and C_s value of 1.5x10^{-3} from six ice categories that are gray young ice, mixture of gray and white ice and leads, rough multi-year ice, step change between ice and water, loose ice fields, and grease ice (Table 2 in their paper). Another parameterization scheme of C_e was developed by Kara et al. (2000) for use in a general circulation model. They related C_e to both surface wind speed and air-sea temperature difference, the fitted expressions are as follows:

$$C_e = C_{e0} + C_{e1} (T_s - T_a) \qquad (26.2)$$
$$C_{e0} = [0.994 + 0.061 \cdot \hat{u} - 0.001 \cdot \hat{u}^2] \cdot 10^{-3} \qquad (26.3)$$
$$C_{e1} = [-0.020 + 0.691 \cdot (1/\hat{u}) - 0.871 \cdot (1/\hat{u})^2] \cdot 10^{-3} \qquad (26.4)$$

where the wind speed is limited to the interval $\hat{u}$ = max[3.0, min(27.5, u)] to suppress the underestimation of the quadratic fit when u > 27.5 m s^{-1}.

Because C_s is so close in value to C_e for sea water, a linear relationship between C_e and C_s is used rather than determining independent C_{s0} and C_{s1} coefficients for the C_s. This relationship also helps to reduce the cost of computing the sensible heat flux as in GCMs. The simplest representative linear formulation is found to be $C_s = 0.96 \cdot C_e$ with a negligible intercept ($3.6 \cdot 10^{-6}$) as reported by Kara et al. (2000); we use $C_s = 0.98 \cdot C_e$ in our model for the air-sea ice interface turbulent heat transfer.

3.4.2.7 Conductive Heat Flux

The seventh term on the left-hand side of the equation (1), F_c, is the conductive heat flux within the ice slab that can be calculated by the following formula as used by Yu and Rothrock (1996).

$$F_c = \gamma (T_f - T_s) \qquad (27)$$

where $\gamma = (k_i k_s) / (k_s h_i + k_i h_s)$, T_f is the water freezing temperature and can be derived from a simplified relationship of $T_f = -0.055 \cdot S_w$, where S_w is the salinity of seawater and assumed to be

31.0 parts per thousand (ppt) for the Beaufort Sea and ***32.5*** ppt for the Greenland Sea, which means T_f is in units of degrees Celsius. h_s is snow depth, and h_i is ice thickness. k_s is the conductivity of snow which can be formulated as $k_s=2.845\cdot10^{-6}\rho_{snow}^{\ 2} + 2.7\cdot10^{-4}\cdot2.0^{(Tsnow-233)/5}$ (Ebert and Curry, 1993), ρ_{snow} is the snow density ranging from ***225*** kg·m^{-3} (new snow) ~ ***450*** kg·m^{-3} (water-soaked snow), T_{snow} is snow temperature in Kelvin. The term k_s can be further simplified as $k_s=2.22362\cdot10^{-5.655}(\rho_{snow})^{1.885}$ (Yen, Y.-C., 1981). Usually, k_s is assumed to be ***0.31*** in some applications. The term k_i is the conductivity of ice that can be estimated by $k_i = k_0 + \beta\cdot S_i/(T_i - 273)$ (Untersteiner's, 1964), where $\beta=0.13$ W·m^{-2}·kg^{-1}, $k_0=2.22\cdot(1-0.00159\cdot T_i)$ W·m^{-1}·K^{-1} is the conductivity of pure ice (Curry and Webster, 1999). S_i is sea ice salinity, T_i is the temperature within the ice slab. Some experimental relative relationships between h_s and h_i, T_i and T_s, S_i and h_i exist as described in the following subsections. See Appendix A for the derivation of Equation 27 for a two-layer system with snow over ice.

3.4.2.7.1 Relationship between Snow Depth and Ice Thickness

Doronin (1971) used the following relationship to estimate snow depth in terms of ice thickness, which was also used in Yu's paper (1996):

$h_s = 0$, for $h_i < 5$ cm;
$h_s = 0.05\cdot h_i$, for $5 \text{ cm} \le h_i \le 20$ cm;
$h_s = 0.1\cdot h_i$, for $h_i > 20$ cm.

In reality, snow accumulation over the ice does not actually obey the relationship above. So we set snow depth as one input variable in the OTIM once climate data or measurements are available.

3.4.2.7.2 Relationship between Surface Temperature and Ice Temperature

The ice temperature T_i is one important factor affecting the ice conductivity calculation, which may be significantly different from the surface skin temperature measured or retrieved with remote sensing data. In general, we can obtain surface skin temperature T_s through satellite retrieval techniques more or less directly, but not T_i if the surface is covered with thick snow. Yu and Rothrock (1996) suggested that assuming T_i is equal to T_s can cause 5% and 1% errors when ice is 5 cm thick and 100 cm thick, respectively. That assumption may be valid at night as during the day most of the solar radiation is reflected back to the atmosphere from the snow layer; during the daylight very little solar radiation actually reaches the interface of the ice and snow, especially for new snow. Thus the surface skin temperature T_s is the surface snow temperature, which may differ significantly from the ice temperature, resulting in a large uncertainty in the ice conductivity calculation, and consequently in a large error in the calculated ice thickness. This uncertainty is one of major error sources for the daytime retrieval of ice thickness with the OTIM. More work should be done to correct the treatment of solar radiation in the OTIM for sunlit conditions.

In addition, if no surface air temperature is available, surface air temperature T_a can be calculated by $T_a = T_s + 2.2 - 1.8C$ where C is the cloud amount (0~1). Furthermore, 90% of surface air relative humidity is assumed when humidity data are not available. Those assumptions and default values were tested to be good estimates from our own work and that of other researchers (Yu and Rothrock, 1996; Persson et al., 2002)

3.4.2.7.3 Relationship between Sea Ice Thickness and Sea Ice Salinity

There are some experimental relationships between sea ice thickness h_i and sea ice salinity S_i as listed below.

1. Cox and Weeks (1974) scheme:

$S_i = 14.24 + 19.39 \cdot h_i$, for $h_i \le 0.4$ m,
$S_i = 7.88 + 1.59 \cdot h_i$, for $h_i > 0.4$ m.

2. Jin, Stamnes, and Weeks (1994) scheme:

$S_i = 7.0 - 31.63 \cdot h_i$, for $h_i \le 0.3$ m,
$S_i = 8.0 - 1.63 \cdot h_i$, for $h_i > 0.3$ m.

3. Kovacs (1996) scheme:

$S_i = 4.606 + 0.91603/h_i$, for $0.10 \text{ m} \le h_i \le 2.0$ m.

We use this scheme in the OTIM.

3.4.2.7.4 Direct Solution from Conductive Heat Flux

If the conductive heat flux F_c is known with other known parameters like k_s and S, the ice thickness can then be retrieved from equation (27) by simply solving the equation, and then the analytical solution can be obtained. Below are the two cases used to solve equation (27) for ice thickness.

1. Fresh Water Ice

For fresh water or lake ice, S_w=0, S_i=0, T_f=*273.15K*, k_i=k_0; therefore it is easy to reorganize equation (27) into the following (28).

Let $T_f - T_s = T_r$, then we have

$$F_c = \frac{k_0 k_s}{k_s h_i + k_0 h_s} T_r \qquad (28)$$

After a series of derivations, we can get the following solution:

$$h_i = \frac{k_0}{F_c} \cdot T_r - \frac{k_0}{k_s} \cdot h_s \qquad (29)$$

2. Sea Ice

From the above discussion, the ice conductivity can be expressed as

$$k_i = \frac{(k_0 T_i - T_0 k_0 + \beta S_0) h_i + \beta S_1}{(T_i - T_0) h_i} \qquad (30)$$

where $S_0=4.606$, $S_1=0.91603$, and $T_0=273.15$.

Let $\boldsymbol{T_i - T_0 = T_k}$, then from Eq. (27) and (30) we have $F_c = \frac{k_i k_s}{k_s h_i + k_i h_s} \cdot T_r$, and letting $a=F_c k_s T_k$, $b=(k_0 T_k+\beta S_0)(F_c h_s-k_s T_r)$, $c=\beta S_1(F_c h_s-k_s T_r)$, $h=h_i$, we have the ice thickness monadic quadratic equation as $ah^2 + bh + c = 0$. Therefore, when $b^2 - 4ac \geq 0$, two real solutions exist as

$$h_1 = \frac{-b + \sqrt{b^2 - 4ac}}{2a}, \text{ and } h_2 = \frac{-b - \sqrt{b^2 - 4ac}}{2a}.$$

When $b^2 - 4ac = 0$, $h_1=h_2$; and when $b^2 - 4ac < 0$, there is no real solution for ice thickness.

3.4.2.8 Solving the OTIM for Ice Thickness

The OTIM can be solved for ice thickness analytically or numerically in terms of input options and variable status as described in the following subsections. First let's rewrite Eq. (1) into the following form

$$(1 - \alpha)(1 - i) F_r + F_c + F = 0 \qquad (31)$$

where $\boldsymbol{F = -F_l^{up} + F_l^{dn} + F_s + F_e - F_a}$, $\alpha = \alpha_s$.

$\alpha = 1 - A_s e^{-B_s h} - C_s e^{-D_s h}$, where h is ice or snow thickness, and A_s, B_s, C_s, D_s are *coefficients* to be determined from Table 2.

$i = A_i e^{-B_i h} + C_i e^{-D_i h}$, where h is ice slab thickness, i is ice slab *transmittance*, and A_i, B_i, C_i, D_i are *coefficients* to be determined from Table 3.

$F_c = r(T_f - T_s)$, $S_i = S_0 + S_1 / h$, let $k_0 T_k + \beta S_0 = g$, we have

$$k_i = \frac{(k_0 T_k + \beta S_0)h + \beta S_1}{T_k h} = \frac{gh + \beta S_1}{T_k h},\ r = \frac{k_s[(k_0 T_k + \beta S_0)h + \beta S_1]}{k_s T_k h^2 + g h_s h + \beta S_1 h_s} = \frac{k_s(gh + \beta S_1)}{k_s T_k h^2 + g h_s h + \beta S_1 h_s},$$

$$F_c = \frac{k_s T_r (gh + \beta S_1)}{k_s T_k h^2 + g h_s h + \beta S_1 h_s}.$$

3.4.2.8.1 Known Surface Albedo and Known Ice Transmittance

If the values of ice/snow surface albedo α and the ice slab transmittance i are both known, let $(1-\alpha)(1-i)F_r + F = F_1$, then we have $F_1 + F_c = 0$, so $F_1 + \frac{k_s T_r (gh + \beta S_1)}{k_s T_k h^2 + g h_s h + \beta S_1 h_s} = 0$

$F_1 k_s T_k h^2 + (F_1 h_s g + k_s T_r g)h + F_1 \beta S_1 h_s + k_s \beta S_1 T_r = 0$, let $a = F_1 k_s T_k$, $b = F_1 h_s g + k_s T_r g$, and

$c = F_1 \beta S_1 h_s + k_s \beta S_1 T_r$, then $h = \frac{-b \pm \sqrt{b^2 - 4ac}}{2a}$, when $b^2 - 4ac \geq 0$, there are real solutions.

3.4.2.8.2 Known Surface Albedo and Unknown Ice Transmittance

If the value of ice surface albedo α is known or snow is present over the ice with a known depth, but the ice slab transmittance i is unknown, let $(1-\alpha)F_r = F_{ra}$, then $(1-i)F_{ra} + F_c + F = 0$.

Let $F + F_{ra} = F_2$, then $F_c - iF_{ra} + F_2 = 0$, so we have

$\frac{k_s T_r (gh + \beta S_1)}{k_s T_k h^2 + \beta S_1 h_s + h_s g h} - F_{ra}(A_i e^{-B_i h} + C_i e^{-D_i h}) + F_2 = 0$; after a series of derivations, we have

$F_{ra}(A_i e^{-B_i h} + C_i e^{-D_i h})(k_s T_k h^2 + g_2 h + k_2 h_s) - [F_2 k_s T_k h^2 + (g k_s T_r + F_2 g_2)h + (k_s T_r + F_2 h_s)k_2] = 0$,

where $k_2 = \beta S_1$, $g_2 = h_s g$. There is no analytical solution for this nonlinear equation; a numerical approach must be applied to solve it for the ice thickness h.

3.4.2.8.3 Unknown Surface Albedo and Known Ice Transmittance

If the value of ice surface albedo α is unknown, but the ice slab transmittance *i* is known, let $(1-i)F_r = F_{ri}$, then $(1-\alpha)F_{ri} + F_c + F = 0$. We know $\alpha = 1-(A_s e^{-B_s h} + C_s e^{-D_s h})$, therefore $F_{ri}(A_s e^{-B_s h} + C_s e^{-D_s h}) + F_c + F = 0$, and $F_c = \dfrac{k_s T_r (gh + k_2)}{k_s T_k h^2 + k_2 h_s + g_2 h}$. Finally, we have $F_{ri}(A_s e^{-B_s h} + C_s e^{-D_s h})(k_s T_k h^2 + g_2 h + k_2 h_s) + F k_s T_k h^2 + (k_s T_r g + F g_2)h + (k_s T_r + F h_s)k_2 = 0$, where $k_2 = \beta S_1$, $g_2 = h_s g$. There is no analytical solution for this nonlinear equation; a numerical approach must be applied to solve it for the ice thickness *h*.

3.4.2.8.4 Unknown Surface Albedo and Unknown Ice Transmittance

If the values of both ice surface albedo α and ice slab transmittance *i* are known, we have $(1-\alpha)(1-i)F_r + F_c + F = 0$, $\alpha = 1-(A_s e^{-B_s h} + C_s e^{-D_s h})$, $i = A_i e^{-B_i h} + C_i e^{-D_i h}$, $F_c = \dfrac{k_s T_r (gh + \beta S_1)}{k_s T_k h^2 + k_2 h_s + g_2 h}$, and $F = -F_l^{up} + F_l^{dn} + F_s + F_e - F_a$. After a series of derivation, $F_r(A_s e^{-B_s h} + C_s e^{-D_s h})(1 - A_i e^{-B_i h} - C_i e^{-D_i h})(k_s T_k h^2 + g_2 h + k_2 h_s) + F k_s T_k h^2 + (k_s T_r g + F g_2)h +$ $(k_s T_r + F h_s)k_2 = 0$, where $k_2 = \beta S_1$, $g_2 = h_s g$. There is no analytical solution for this nonlinear equation; a numerical approach must be applied to solve it for the ice thickness*h*.

3.4.2.8.5 Nighttime Solution

At night, there is no need to consider solar radiation in the OTIM, so we can set $F_r = 0$, therefore from $(1-\alpha)(1-i)F_r + F_c + F = 0$, we have $F_c + F = 0$, and we know $F_c = \frac{k_s T_r (gh + k_2)}{k_s T_k h^2 + k_2 h_s + g_2 h}$, so $\frac{k_s T_r (gh + \beta S_1)}{k_s T_k h^2 + k_2 h_s + g_2 h} + F = 0$. Finally we have

$$F k_s T_k h^2 + (k_s T_r g + F g_2) h + (k_s T_r + F h_s) k_2 = 0$$

Let $a = F k_s T_k$, $b = k_s T_r g + F g_2$, $c = (k_s T_r + F h_s) k_2$, then we have $ah^2 + bh + c = 0$, so the solution for the monadic quadratic equation is $h = \frac{-b \pm \sqrt{b^2 - 4ac}}{2a}$, and when $b^2 - 4ac \geq 0$, there are real solutions.

3.4.2.9 Ice Age

The GOES-R Mission Requirements Document (MRD) requires, at the Threshold level, that ice-free areas be distinguished from first-year ice and older ice areas. The Goal requirement is to distinguish not only ice-free from first-year ice areas, but also to distinguish between the following types of ice: nilas, grey white, first-year medium, first-year thick, second-year, multiyear smooth, and multiyear deformed, commonly called ice age. Generally speaking, older ice is thicker than younger ice. As this assumption is considered valid as tested and verified by many other researchers (e.g., Tucker et al., 2001; Yu et al., 2004; Maslanik et al., 2007), ice thickness is used as a proxy for ice age.

There is internationally accepted terminology for ice form and conditions, coordinated by the WMO. This terminology is used by the Canadian Ice Service as the basis for reporting ice conditions, and adopted by this work, with minor modifications, for classifying ice into different categories. Refer to the *Manual of Standard Procedures for Observing and Reporting Ice Conditions* by the Canadian Ice Service, available at http://ice-glaces.ec.gc.ca/App/WsvPageDsp.cfm?Lang=eng&lnid=23&ScndLvl=no&ID=172.

Sea-ice types

- **New**: A general term for recently formed ice which includes frazil ice, grease ice, slush and shuga. These types of ice are composed of ice crystals which are only weakly frozen together (if at all) and have a definite form only while they are afloat.
- **Nilas**: A thin elastic crust of ice, easily bending on waves and swell and under pressure growing in a pattern of interlocking “fingers” (finger rafting). Nilas has a matte surface and is ***up to 10 cm*** in thickness and may be subdivided into dark nilas and light nilas.
- **Grey Ice**: Young ice ***10-15 cm*** thick. Less elastic than nilas and breaks on swell. Usually rafts under pressure.
- **Grey-white Ice**: Young ice ***15-30 cm*** thick. Under pressure it is more likely to ridge than to raft.
- **Thin First-year Ice**: First-year ice of not more than one winter's growth, ***30-70 cm*** thick.

- **Medium First-year Ice**: First-year, ice ***70-120 cm*** thick.
- **Thick First-year Ice**: First-year ice ***120-170 cm*** thick.
- **Old Ice**: Sea ice which has survived at least one summer's melt. Topographic features generally are smoother than first-year ice, and ***more than 170 cm*** thick. May be subdivided into second-year ice and multi-year ice.
- **Second-year Ice**: Old ice which has survived only one summer's melt.
- **Multi-year Ice**: Old ice which has survived at least two summer's melt.

Lake-ice types

- **New**: Recently formed ice ***less than 5 cm*** thick.
- **Thin**: Ice of varying colors, ***5-15 cm*** thick.
- **Medium**: A further development of floes or fast ice, ***15-30 cm*** thick.
- **Thick**: Ice ***30-70 cm*** thick.
- **Very Thick**: Floes or fast ice developed to ***more than 70 cm*** thickness.

3.4.3 Algorithm Output

The final outputs of this algorithm are ice thickness, ice age, and other optional parameters (Tables 5 and 6). The ice thickness values are in the range 0 to > 3.0 m for both sea ice and lake ice. Ice age categories and descriptions of their meanings are given in Table 5. The associated ice thickness and age quality flags (Table 7) and metadata information are also provided and described here.

Table 5. AITA output parameters and their definitions.

Definition	**Description**
Ice Thickness	Ice thickness is defined as the total vertical length of the ice under and above the water surface. The reliable ice thickness retrieved from this algorithm ranges between ***0 ~ 3.0 m***.
Ice age	
1: New	Recently formed ice which includes frazil ice, grease ice, slush and shuga. These types of ice are composed of ice crystals which are only weakly frozen together (if at all) and have a definite form only while they are afloat, usually less than 2 cm in thickness.
2: Nilas	A thin elastic crust of ice, easily bending on waves and swell and under pressure growing in a pattern of interlocking “fingers” (finger rafting). Nilas has a matte surface and is ***up to 10 cm*** in thickness and may be subdivided into dark nilas and light nilas.
3: Grey	Young ice ***10-15 cm*** thick. Less elastic than nilas and breaks on swell. Usually rafts under pressure.
4: Grey-white	Young ice ***15-30 cm*** thick. Under pressure it is more likely to ridge than to raft.

5: First-year Thin	First-year ice of not more than one winter's growth, ***30-70 cm*** thick.
6: First-year Medium	First-year, ice ***70-120 cm*** thick.
7: First-year Thick	First-year ice ***120-170 cm*** thick.
8: Older Ice	Sea ice which has survived at least one summer's melt. Topographic features generally are smoother than first-year ice, and ***more than 170 cm*** thick. May be subdivided into second-year ice and multi-year ice using *Lagrangian* tracking technique developed by Fowler and Maslanik (2004), not OTIM. **Second-year Ice**: Old ice which has survived only one summer's melt. **Multi-year Ice**: Old ice which has survived at least two summer's melt.

The algorithm can also output other optional parameters that are closely related to the surface energy budget and ice thickness retrieval. These optional outputs from OTIM are listed and described in Table 6. These optional output parameters will be implemented in the next version of the algorithm.

Table 6. AITA optional output parameters and their definitions.

Parameter	**Unit**	**Description**
Cloud mask	0 or 1	Clear or cloudy over the ice surface, observed.
Surface broadband albedo	0 ~ 1	Ice/snow surface broadband albedo, modeled or in-situ measured, daytime only.
Ice transmittance	0 ~ 1	Ice slab transmittance for solar radiation, modeled or measured, daytime only.
Surface incoming solar radiation flux	$W \cdot m^{-2}$	Incoming solar radiation flux at the surface, modeled or observed, daytime only.
Surface outgoing thermal radiation flux	$W \cdot m^{-2}$	Outgoing thermal radiation flux at the surface, modeled or observed.
Surface incoming thermal radiation flux	$W \cdot m^{-2}$	Incoming thermal radiation flux at the surface, modeled or observed.
Surface turbulent sensible heat flux	$W \cdot m^{-2}$	The turbulent sensible heat flux at the interface of ice and the above atmosphere, modeled or observed.
Surface turbulent latent heat flux	$W \cdot m^{-2}$	The turbulent latent heat flux at the interface of ice and the above atmosphere, modeled or observed.
Conductive heat flux	$W \cdot m^{-2}$	Conductive heat flux within the ice slab.
Other potential optional output parameters:		
Surface skin temperature	K	Ice/snow surface skin temperature, observed.

Surface air temperature	K	Surface air temperature at 2 m above the ground, modeled or observed.
Surface air humidity	0%~100%	Surface air humidity, relative or mixing ratio, modeled or observed.
Surface wind	$m \cdot s^{-1}$	Surface wind speed at 2 m above the ground, observed.
Sea water salinity	PPT	Sea water salinity, modeled or observed.
Sea ice salinity	PPT	Sea ice salinity, modeled or observed.
Snow depth	m	Snow accumulation over the ice in meter, modeled or observed.
Water freezing point	K	The temperature at which water freezes, modeled or observed.
Snow conductivity	$W \cdot m^{-1} \cdot K^{-1}$	Snow conductivity, modeled or observed.
Ice conductivity	$W \cdot m^{-1} \cdot K^{-1}$	Ice conductivity, modeled or observed.

Table 7. AITA products quality information (4 bytes)[*].

Byte	Bit	Quality Flag Name	Description	Meaning
0	0 1	QC_OUTPUT	Output product quality	00 - normal 01 - uncertain 10 – non-retrievable 11-bad data
	2 3	QC_INPUT_CLD	cloud mask	00 - clear 01 - probably clear 10 -probably cloudy 11-cloudy
	4	QC_INPUT_DAY	Day/Night	0-Day 1-Night
	5	QC_INPUT_SUNGLINT	Sunglint or not	0-Yes 1-No
	6	QC_INPUT_CLDSHADOW	Cloud shadow or not	0-Yes 1-No
	7	QC_INPUT_ICEIDEN	Ice identification	0-Yes 1-No
1	0	QC_INPUT_ICECONC	Ice concentration	0-Yes 1-No
	1	QC_INPUT_ICETRAN	Ice transmittance	0-Yes 1-No
	2	QC_INPUT_SOLZEN	Valid solar zenith angle	0-Yes 1-No
	3	QC_INPUT_SATZEN	Valid satellite zenith angle	0-Yes 1-No
	4	QC_INPUT_ALBEDO	Surface broadband albedo	0-Yes 1-No
	5	QC_INPUT_TSURF	Surface skin temperature	0-Yes 1-No
	6	QC_INPUT_SNOW	Surface snow depth	0-Yes 1-No
	7	QC_INPUT_WIND	Surface wind speed	0-Yes 1-No
2	0 1	QC_INPUT_SURFACE	Surface background flag	00 - in-land water 01 - sea water 10- land 11 - others
	2	QC_INPUT_TAIR	Surface air temperature	0-Yes 1-No
	3	QC_INPUT_PRESSURE	Surface air pressure	0-Yes 1-No

	4	QC_INPUT_HUMIDITY	Surface air relative humidity	0-Yes 1-No
	5	QC_INPUT_SSWD	Surface shortwave downward radiative flux	0-Yes 1-No
	6	QC_INPUT_SLWD	Surface longwave downward radiative flux	0-Yes 1-No
	7	QC_INPUT_SLWU	Surface longwave upward radiative flux	0-Yes 1-No
3	0	QC_INPUT_SSHF	Surface turbulent sensible heat flux	0-Yes 1-No
	1	QC_INPUT_SLHF	Surface turbulent latent heat flux	0-Yes 1-No
	2	QC_INPUT_SCHF	Surface conductive heat flux	0-Yes 1-No
	3	QC_INPUT_SRHF	Surface residual heat flux	0-Yes 1-No
	4	QC_RET_ALGO	Day/Night algorithm selection	0-Day 1-Night
	5	QC_RET_METH	Math method for solution	0-Analytical 1-Numerical
	6	QC_RET_RESU	Retrieval success or fail	0-Success 1-Fail
	7			

*: The ”Yes/No” flag indicates whether or not that input parameter is available. Some input parameters must be given in order to do ice thickness/age retrieval; these critical input parameters include cloud mask, solar zenith angle, surface skin temperature, ice identification. Other input parameters can be missing or not available for input, so-called optional able-to-missing parameters, that will result in the default values of those parameters being assigned or calculated by OTIM built-in parameterization schemes; these parameters include surface air temperature, humidity, pressure, and wind speed, surface broadband albedo, ice slab transmittance, cloud shadow, ice concentration, satellite zenith angle, day/night indicator, sunglint mask, and all shortwave and longwave radiation fluxes.

The metadata are also included in the final products. The metadata include the common metadata for all data products and specific metadata for ice thickness and age products.

Common metadata for all data products:

- DateTime (swath beginning and swath end)
- Bounding Box
  - Product resolution (nominal and/or at nadir)
  - Number of rows, and number of columns
  - Bytes per pixel
  - Data type
  - Byte order information
  - Location of box relative to nadir (pixel space)
- Product Name
- Product units

- Ancillary data to produce product (including product precedence and interval between datasets is applicable)
  - Version Number
  - Origin
  - Name
- Satellite
- Instrument
- Altitude
- Nadir pixel in the fixed grid
- Attitude
- Latitude, longitude
- Grid projection
- Type of scan
- Product version number
- Data compression type
- Location of production
- Citations to documents
- Contact information

Ice Thickness and Age Specific Metadata:

- Number of QA flag values (currently, there are 4: Normal or Optimal; Uncertain or Suboptimal; Non-retrievable; Bad or missing)
- For each QA flag value, the following information is provided:
  - Definition of QA flag
  - Total pixel numbers with the QA flag
- Total number of pixels with water surface
- Total number of valid ice thickness and age retrievals (normal + uncertain)
- Total percentage of valid ice thickness and age retrievals of all pixels with water surface
- Total pixels numbers and percentage of terminator pixels (Non-retrievable and Bad)
- Pixel number of daytime ice thickness and age valid retrievals
- Pixel number of nighttime ice thickness and age valid retrievals
- Mean, Min, Max, and standard deviation of valid ice thickness retrievals

4 Test Data Sets and Outputs

4.1 Simulated/Proxy Input Data Sets

The simulated/proxy input data sets used to test the AITA included APP-x, MODIS, and SEVIRI observations as detailed in the following subsections.

4.1.1 APP-x Data

The Advanced Very High Resolution Radiometer (AVHRR) Polar Pathfinder (APP) project (Fowler, et al, 2002) recently produced 23 years of twice-daily, bi-polar surface temperature, surface albedo, and cloud information products. The APP data has been extended to include cloud properties and surface radiative fluxes (Wang and Key, 2003). The extended AVHRR Polar Pathfinder data set, called the APP-x data set, covers the entire Arctic and Antarctica area and spans 1982-2004 at a spatial resolution of 25 km. Specifically, the data we are interested in for this work are cloud information, surface skin temperature, surface broadband albedo, and surface radiation fluxes retrieved from satellite observations as inputs to the OTIM for estimating ice thickness and age along with other ancillary profile data and wind data from NCAR/NCEP. Figure 2 is an example of AITA retrieved monthly ice thickness and ice age with APP-x data.

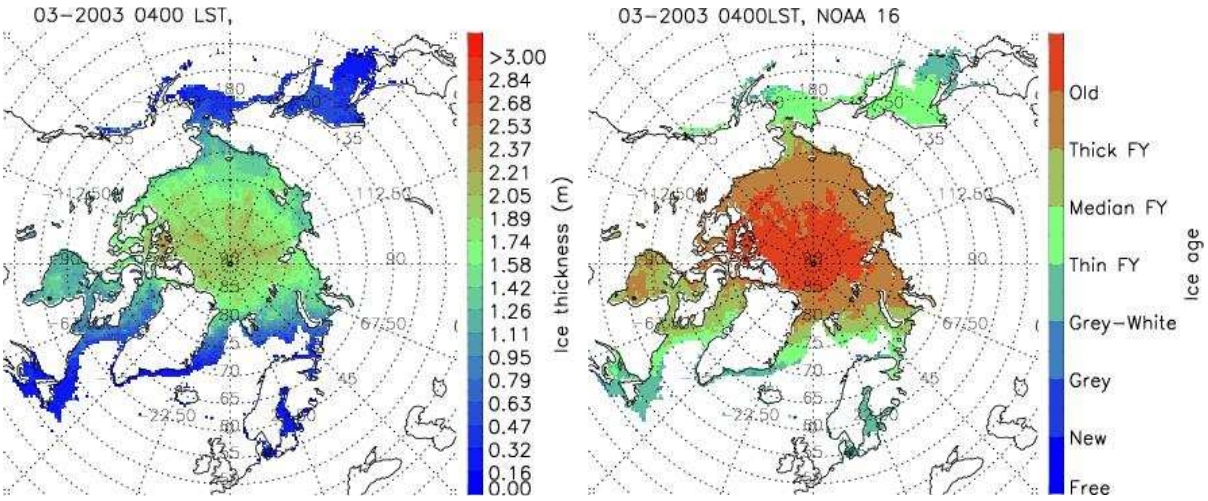

Figure 2. AITA retrieved monthly mean ice thickness (left) and ice age (right) with APP-x data for March 2003 under all sky condition.

4.1.2 MODIS Data

MODIS (Moderate Resolution Imaging Spectroradiometer) is a key instrument aboard the Terra (*EOS AM, refer to http://terra.nasa.gov/*) and Aqua (*EOS PM, refer to http://aqua.nasa.gov/*) satellites. Terra's orbit around the Earth is timed so that it passes from north to south across the equator in the morning, while Aqua passes south to north over the equator in the afternoon. The MODIS instrument has a viewing swath width of 2,330 km and views the entire surface of the Earth every one to two days. Its detectors measure 36 spectral bands between 0.405 and 14.385 μm, and it acquires data at three spatial resolutions: 250m, 500m, and 1,000m. Many data products derived from MODIS observations describe features of the land, oceans and the atmosphere that can be used for studying processes and trends on local to global scales to improve our understanding of global dynamics and processes occurring on land, in the oceans, and in the lower atmosphere. MODIS plays a vital role in the development of validated, global, interactive Earth system models able to predict global change accurately enough to assist policy

makers in making sound decisions concerning the protection of our environment. Figure 3 and 4 show two cases of AITA retrieved daily ice thickness and ice age with MODIS data.

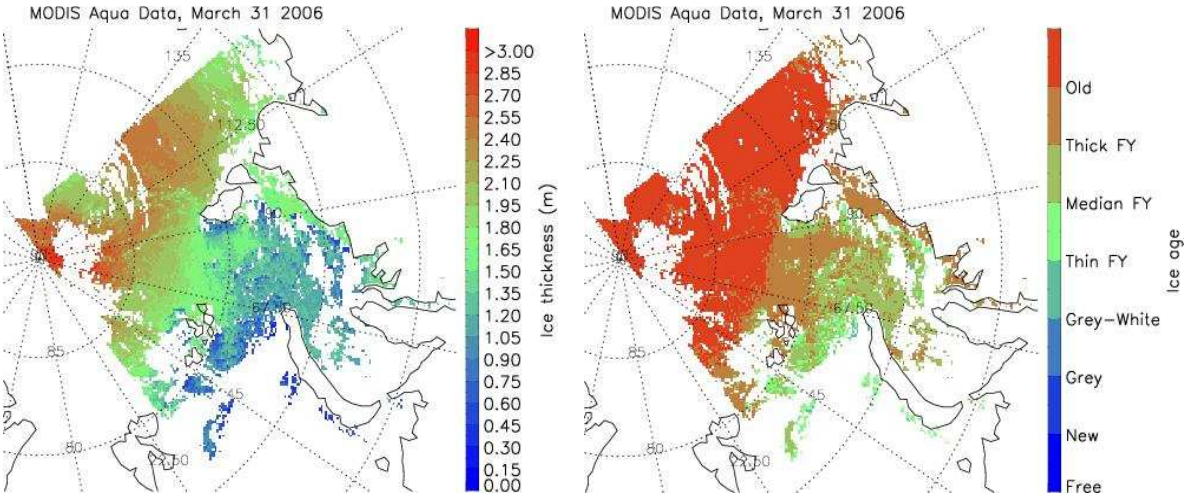

Figure 3. AITA retrieved ice thickness (left) and ice age (right) with MODIS Aqua data on March 31, 2006 under clear sky conditions.

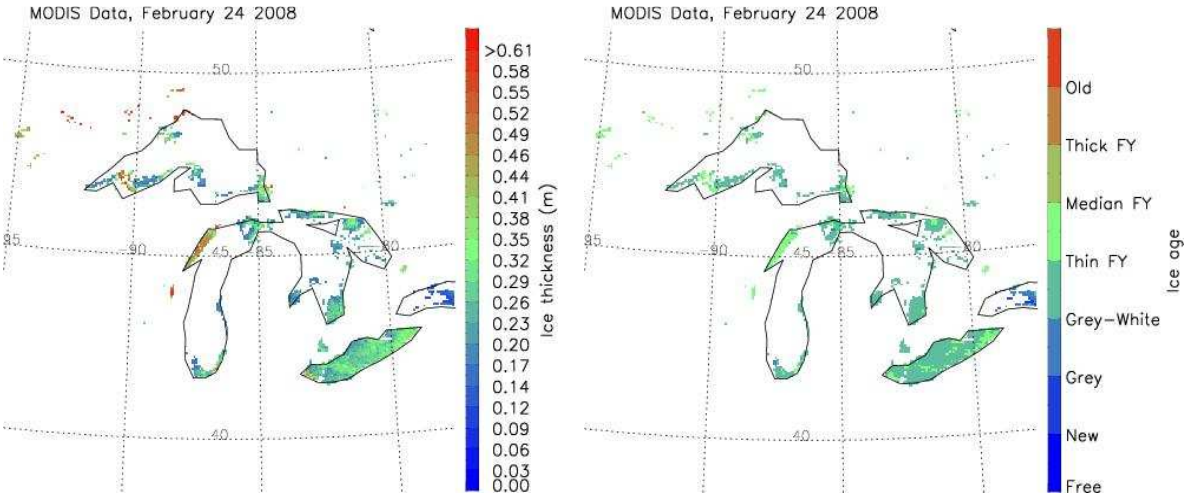

Figure 4. AITA retrieved ice thickness (left) and ice age (right) with MODIS Aqua data on February 24, 2008 under clear sky conditions.

4.1.3 SEVIRI Data

SEVIRI (Spinning Enhanced Visible & InfraRed Imager) is the primary payload of the MSG (Meteosat Second Generation) satellites which have been a joint project between the European Space Agency and EUMETSAT (the European Organisation for the Exploitation of Meteorological Satellites) since 1977 (*refer to http://www.eumetsat.int/home/Main/Access_to_Data/Meteosat_Image_Services/SP_1123237865326*). SEVIRI measures reflected and emitted radiance in 11 spectral channels located between 0.6 μm and 14 μm with a nominal spatial resolution of 3 km at the sub-satellite point alone with an additional broadband high-resolution visible (HRV, 0.4-1.1 μm) channel that has 1 km spatial resolution. The full disk view allows frequent sampling, every 15 minutes, enabling monitoring of rapidly evolving events. The nominal coverage includes all of Europe, all of Africa and locations at which the elevation to the satellite is greater than or equal to 10^{o} (Figure 5). Figure 6 shows one case of AITA retrieved daily ice thickness and ice age with SEVIRI data.

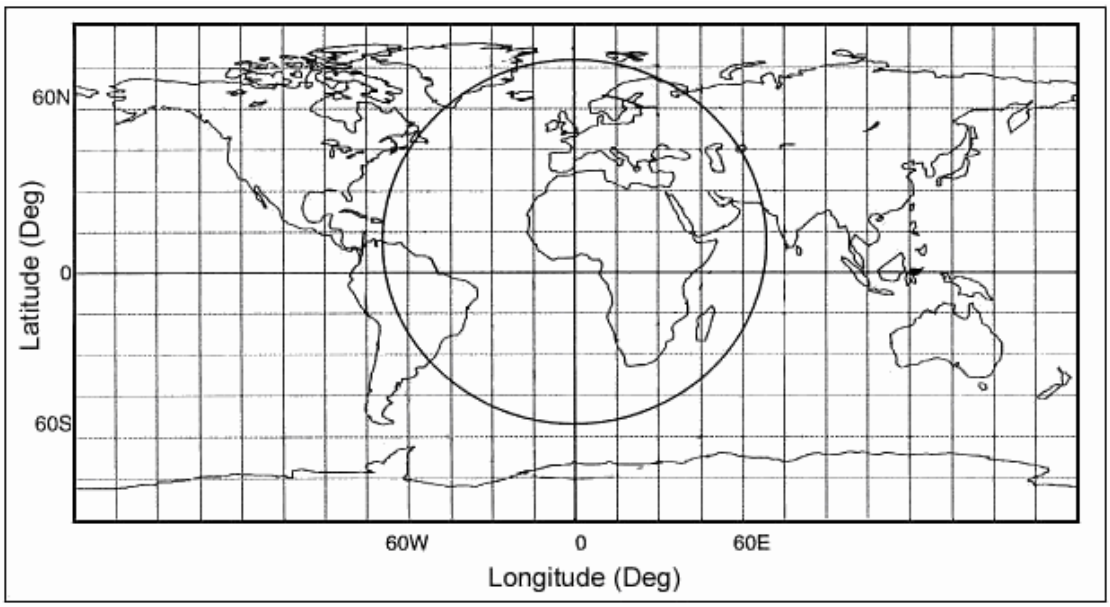

Figure 5. MSG Telecommunications coverage area.

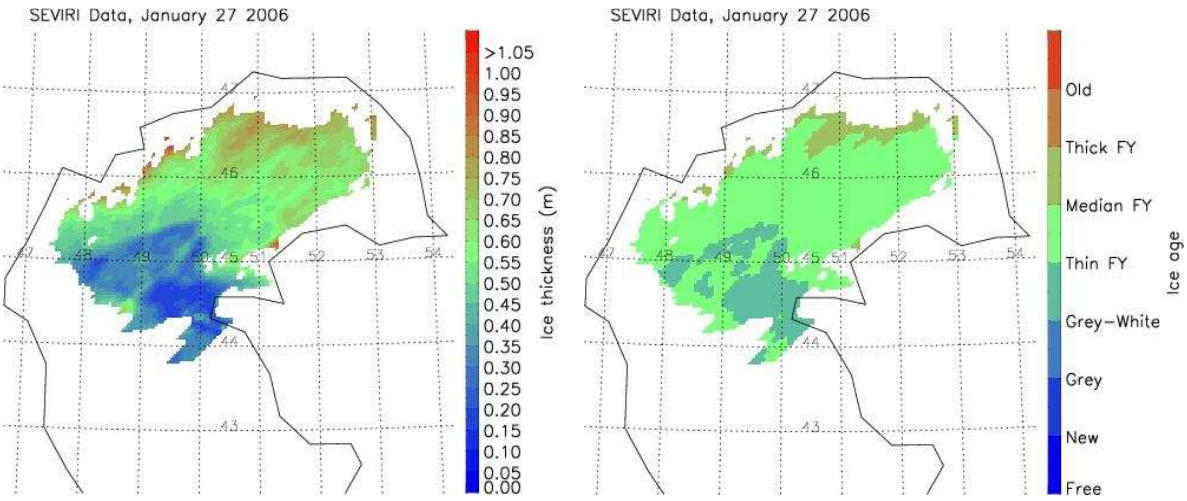

Figure 6. AITA retrieved ice thickness (left) and ice age (right) with SEVIRI data on January 27, 2006 under clear sky conditions.

4.2 Output from Simulated Input Data Sets

The output results from proxy data sets with the AITA algorithm are given in Figures 2, 3, 4, and 6 in the previous section.

4.2.1 Precisions and Accuracy Estimates

To estimate the performance of the AITA, we have used comprehensive numerical model simulations, submarine and moored Upward Looking Sonar (ULS) measurements, and meteorological station measurements to assess and validate the AITA. This section will present our analysis methodology for estimating the precision and accuracy. The next section will provide the quantitative results in terms of the MRD specifications.

4.2.1.1 Numerical Model Simulation Analysis

For this project the Pan-Arctic Ice-Ocean Modeling and Assimilation System (PIOMAS) was used for validation purposes. PIOMAS is a coupled Parallel Ocean and sea Ice Model (POIM, Zhang and Rothrock 2003) capable of assimilating ice concentration and velocity data. It is formulated in a generalized orthogonal curvilinear coordinate (GOCC) system and designed to run on computers with a single processor or massively parallel processors. PIOMAS couples the Parallel Ocean Program (POP), developed at the Los Alamos National Laboratory, with a thickness and enthalpy distribution (TED) sea-ice model, which is a dynamic thermodynamic model that also explicitly simulates sea-ice ridging. The TED model originates from the

Thorndike et al. (1975) thickness distribution theory and is recently enriched by enthalpy distribution theory (Zhang and Rothrock, 2001).

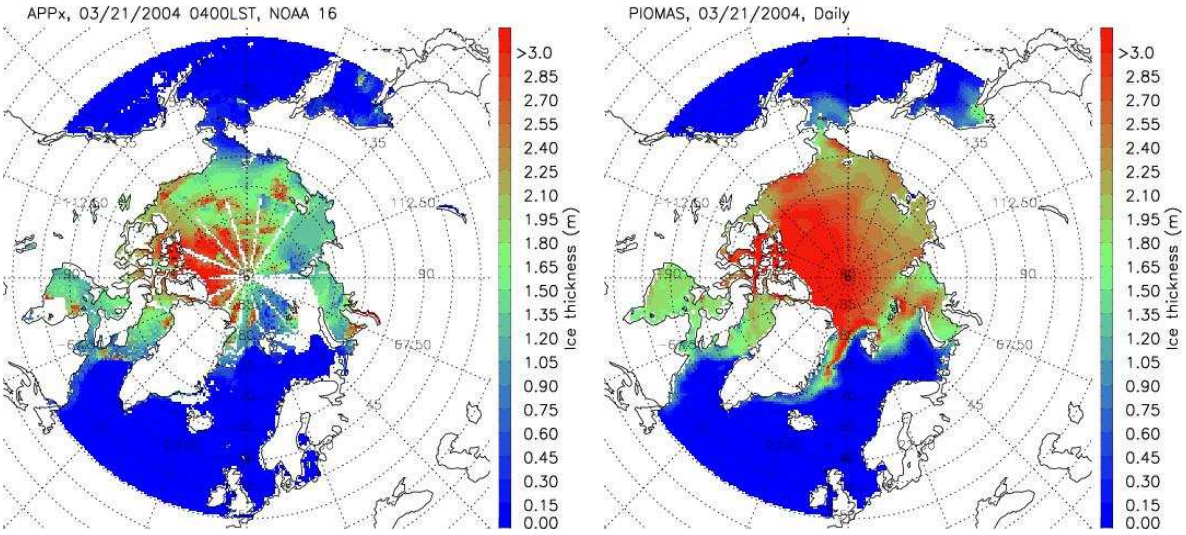

Figure 7. AITA retrieved ice thickness (left) with APP-x data and PIOMAS simulated ice thickness (right) for March 21, 2004 under all sky conditions.

The PIOMAS data sets from the retrospective investigation include model output for 1978-2005, specifically estimates of some key ice and ocean variables. The data sets only include results for the period of 1978-2005 when satellite ice concentration data are available for assimilation. These data sets include Arctic sea ice thickness and concentration, snow depth, ice growth rate, ocean surface salinity, and others. Of special interest to this work is the PIOMAS estimated sea ice thickness. Figure 7 shows the AITA estimated Arctic sea ice thickness with APP-x data and the PIOMAS estimation on the same day March 21, 2004. Overall, AITA estimated sea ice is thinner than PIOMAS; the inconsistency or mismatch will be investigated in the next section with submarine cruise measurements and in-situ station measurements.

4.2.1.2 Submarine Cruise Measurement Analysis

National Snow and Ice Data Center (NSIDC) archive data come from theSubmarine Upward Looking Sonar Ice Draft Profile Data and Statistics over recent decades. This data set consists of upward looking sonar draft data collected by submarines in the Arctic Ocean. Data are provided as ice draft profiles and as statistics derived from the profile data. Statistics files include information concerning ice draft characteristics, keels, level ice, leads, undeformed and deformed ice (refer to http://nsidc.org/data/g01360.html). This data set includes submarine data collected in the Arctic Ocean by U.S. Navy and Royal Navy submarines. U.S. Navy guidance has stated that previously classified, submarine-collected ice draft data may be declassified and released according to set guidelines. Those guidelines include restrictions stating that data

positions must be rounded to the nearest 5 minutes of latitude and longitude, and the date is to be rounded to the nearest third of a month. Due to the limitations enforced by those guidelines for temporal and spatial information, not all of the data are suitable to be used by scientific study.

Fortunately, not all data from U.S. Navy submarines are restricted. Data from a research program called Scientific Ice Expeditions (SCICEX), using a U.S. Navy submarine, are not classified and do not have restrictions on reporting the precise location and date; in fact, the SCICEX ice draft data in this collection are reported with their date of acquisition, and the position is reported to six decimal places, which make the SCICEX data suitable for scientific study (Figure 8). We used SCICEX 1999 ice draft data (hereafter SCICEX-99) in this work because NSIDC obtained permission to release some SCICEX-99 data acquired outside the previously mentioned release box, meaning a larger area of coverage for the data set. There are two types of data files, one for ice draft profiles, and the other for statistics derived from the profile data. Ice draft files include a header that provides the date and location information followed by a sequential list of drafts spaced at 1.0 m intervals that comprise the bottom-side sea-ice roughness profile. Data in each file fall along a straight-line (great circle) track between the two end points given in the header. The length of the profile in any given file can be up to 50 km, but may be shorter if data dropouts create gaps greater than 0.25 km, or if changes in course cause deviations from a straight-line track. Statistics files include information on ice draft characteristics, keels, level ice, leads, and un-deformed and deformed ice.

Figure 9 and 10 show the comparisons of the three data sets (APP-x, submarine, and PIOMAS) with regard to ice thickness. Results are given in Table 8. Note the submarine actually measures ice draft (ice below the surface), which is roughly 89% of the total ice thickness based on Archimedes' buoyancy principle in terms of different water and ice densities. The draft can be approximately converted to thickness using an empirical multiplicative factor of 1.11

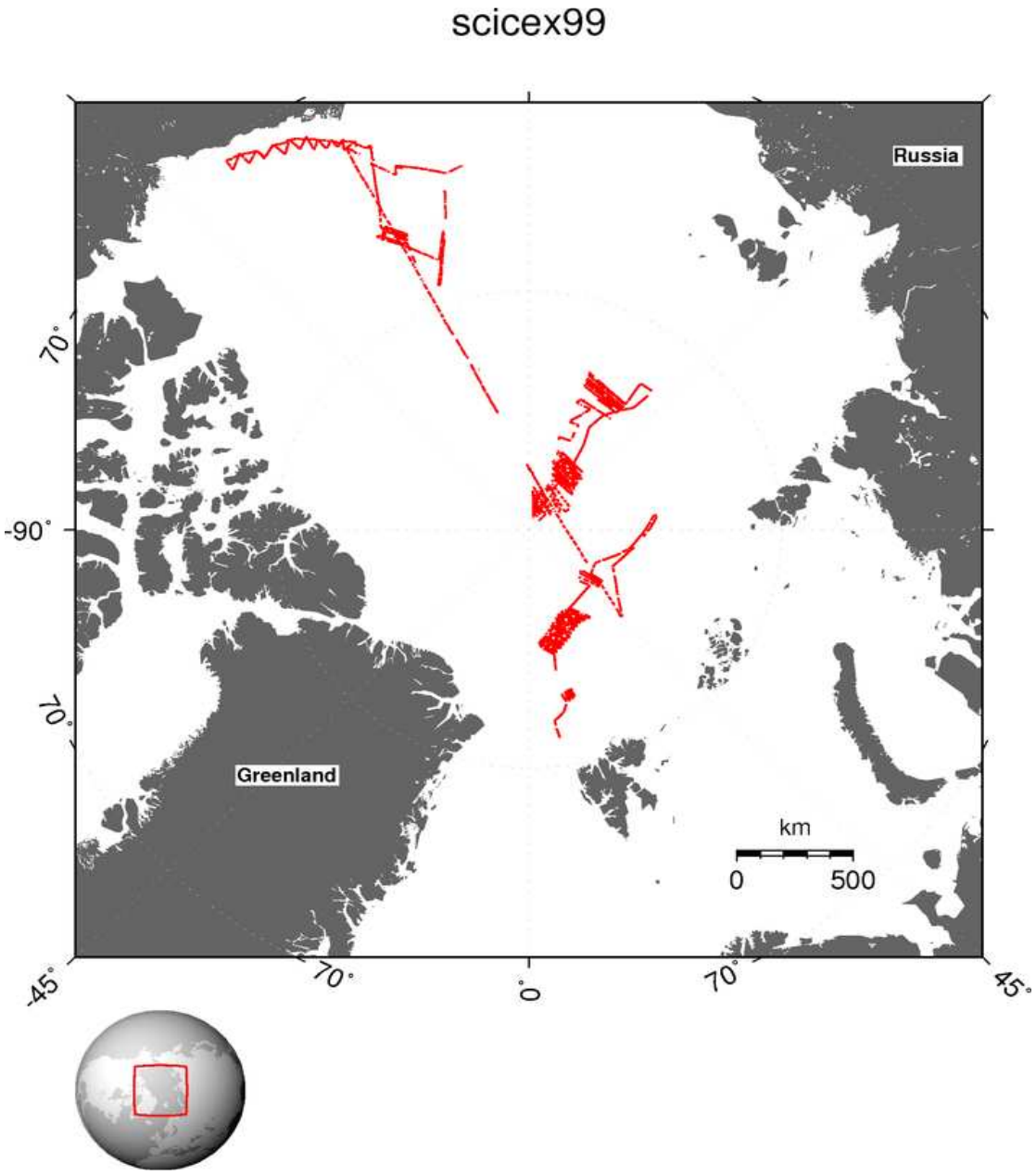

Figure 8. U.S. Navy submarine track for SCICEX ice draft data collection during April 2 – May 13 in 1999.

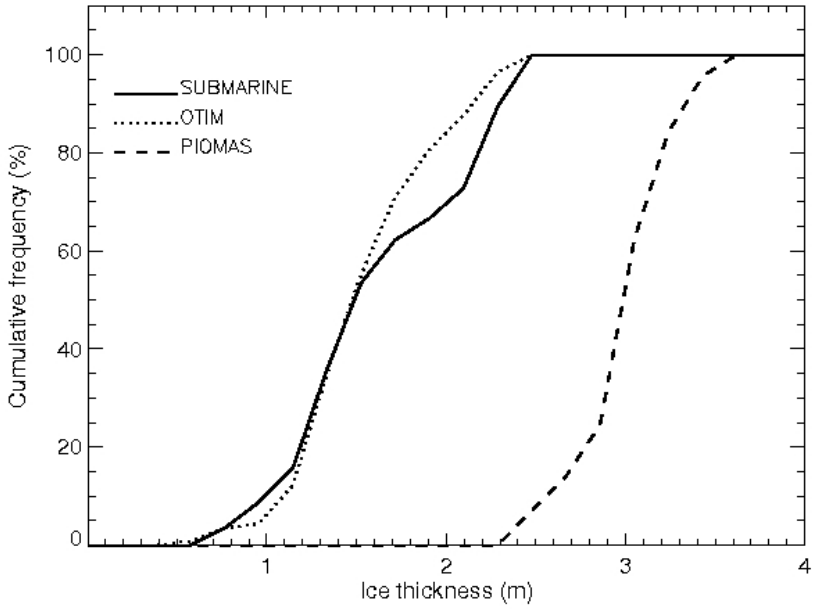

Figure 9. Comparisons of ice thickness cumulative distribution retrieved by OTIM with APP-x data, measured by submarine, and simulated by the numerical model PIOMAS. Submarine ice draft (mean and median only) was already converted to ice thickness using a factor of 1.11.

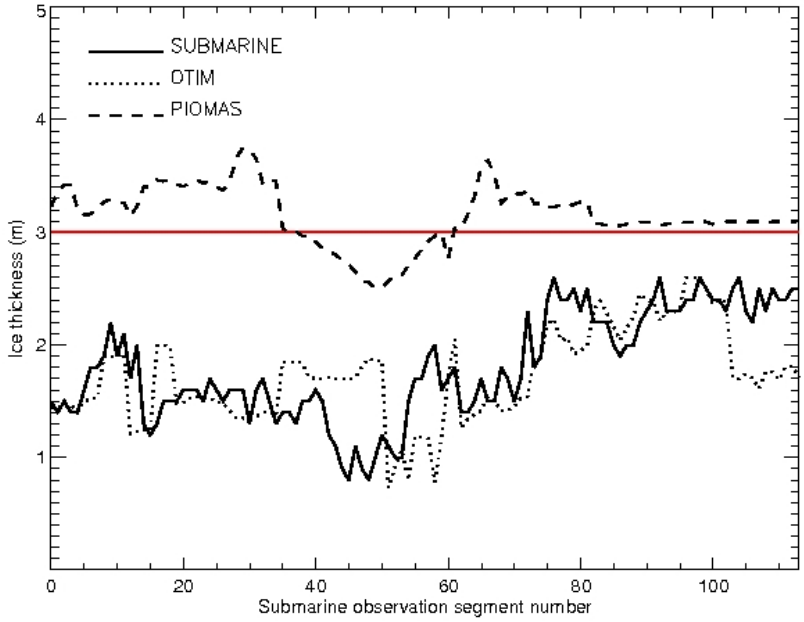

Figure 10. Comparisons of ice thickness values retrieved by OTIM with APP-x data, measured by submarine, and simulated by the numerical model PIOMAS along the submarine track segments. Submarine ice draft (mean and median only) was already converted to ice thickness using a factor of 1.11.

Table 8. The AITA validation result against submarine measurements.

	AITA	Submarine
Thickness Mean (m)	1.73	1.80
Bias Mean (m)	-0.07	
Bias Absolute Mean (m)	0.31	
Bias Standard Deviation	0.42	
Accuracy*	83%	
AITA Ice Age	Ice free water, new/fresh, nilas, grey, grey-white, first year thin, first year medium, first year thick, and multi-year ice.	
ADR Requirements	Distinguish between ice free areas, first-year ice, and older ice.	
CDR Requirements	Distinguish between Ice free, new/fresh ice, nilas, grey white, first Year medium, first Year Thick, second year, and multiyear smooth and deformed ice.	

***** *Accuracy=(1.0 – (Bias Absolute Mean)/(Submarine Mean Ice thickness))*%*

4.2.1.3 Station Measurement Analysis

The Canadian Ice Service (CIS) maintains archived Ice Thickness and On-Ice Snow Depth Measurements for Canadian Stations (Figure 11) back as far as 1947 for the first established stations in the Canadian Arctic (Eureka and Resolute). By the beginning of 2002 most stations from the original Ice Thickness program had stopped taking measurements. Fortunately, due to an increasing interest in updating this historical dataset to support climate change studies, a new program was started in the fall of 2002, called the New Arctic Program (refer to http://ice-glaces.ec.gc.ca/App/WsvPageDsp.cfm?Lang=eng&lnid=5&ScndLvl=no&ID=11703). Several stations in the Canadian Arctic were re-opened and started taking measurements. These New Arctic Program stations are listed in Table 9. The New Arctic Program Data will be used in this work.

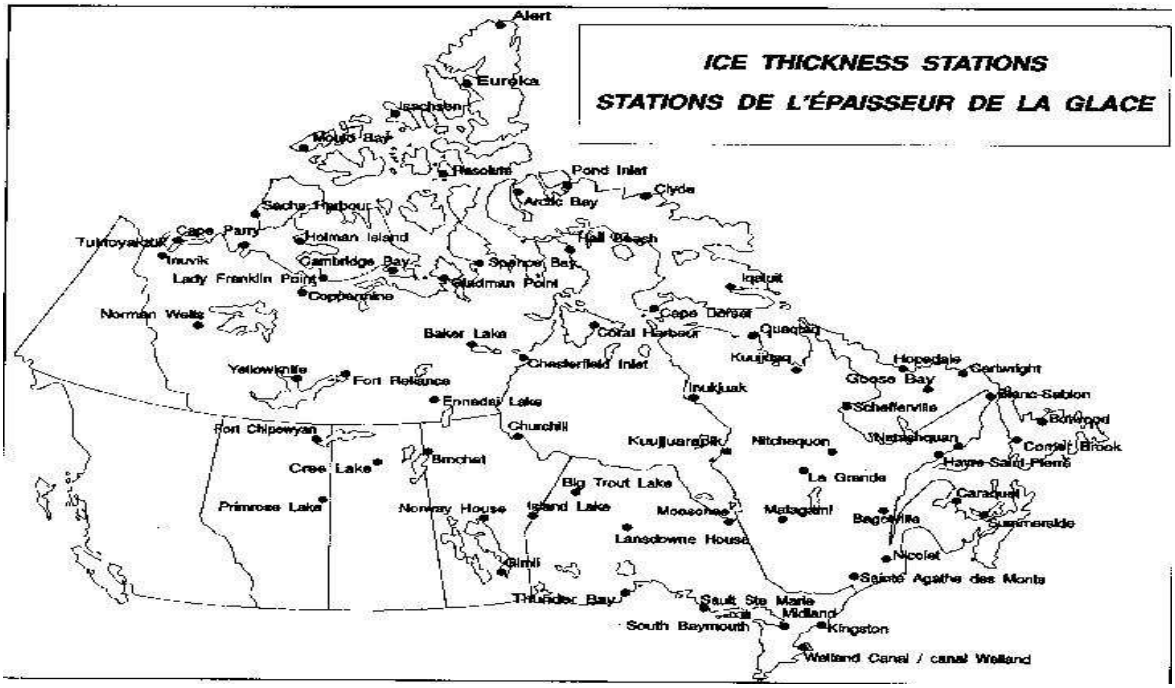

Figure 11. Spatial deployment of the Canadian stations for ice thickness and on-ice snow depth measurements.

Table 9. Geographic Information of the New Arctic Program Stations (Starting Fall 2002) for Ice Thickness and On-Ice Snow Depth Measurements.

Station ID	Station Name	Start Date	LAT	LON
LT1	ALERT LT1	10/16/2002	82.466667	-61.5
YLT	ALERT YLT	10/16/2002	82.500275	-61.716667
YBK	BAKER LAKE YBK	11/27/2002	64.316666	-95.966667
YCB	CAMBRIDGE BAY YCB	12/07/2002	69.10833	-104.95
YZS	CORAL HARBOUR YZS	11/15/2002	64.119446	-82.741669
WEU	EUREKA WEU	10/11/2002	79.986115	-84.099998
YUX	HALL BEACH YUX	11/10/2002	68.765274	-80.791664
YEV	INUVIK YEV	11/29/2002	68.35833	-132.26138
YFB	IQALUIT YFB	01/04/2003	63.727779	-67.48333
YRB	RESOLUTE YRB	12/13/2002	74.676941	-93.131668
YZF	YELLOWKNIFE YZF	11/29/2002	62.465556	-114.36556

Most of the data in the current archive at the Canadian Ice Service have been collected by the Atmospheric Environment Program of Environment Canada, but some data are provided by other organizations such as the St-Lawrence Seaway Authority, Trent University and Queen's University. Measurements are taken approximately at the same location every year on a weekly basis starting after the initial freeze when the ice is safe to walk on, and continuing until break-up or when the ice becomes unsafe. The location is selected close to shore, but over a depth of water which will exceed the maximum ice thickness. Ice thickness is measured to the nearest centimeter using either a special auger kit or a hot wire ice thickness gauge. The depth of snow on the ice at the location of ice thickness measurement is also measured and reported to the nearest centimeter. Measurements after 1982 include additional information (coded values as per code for additional information at bottom) such as character of ice surface, water features and method of observation. Figures 12 and 13 show the comparisons of the three data sets for ice thickness in cumulative frequency and in absolute magnitude, respectively. Results are given in Table 10.

Table 10. The AITA validation result against in-situ station measurements.

AITA Station	**AITA ALERT LT1**	**AITA ALERT YLT**	**AITA CAMBRIDGE BAY YCB**	**AITA CORAL HARBOUR YZS**	**AITA EUREKA WEU**	**AITA HALL BEACH YUX**	**AITA RESOLUTE YRB**	**AITA YELLOWKNIFE YZF**
Thickness Mean (m)	1.17 1.23	1.21 1.26	1.48 1.51	1.17 1.20	1.36 1.54	1.37 1.46	1.21 1.50	0.91 0.93
Bias Mean (m)	-0.06	-0.06	-0.04	-0.03	-0.18	-0.07	-0.29	-0.01
Bias absolute Mean (m)	0.14	0.16	0.58	0.32	0.27	0.32	0.31	0.31
AITA Ice Age	Ice free water, new/fresh, nilas, grey, grey-white, first year thin, first year medium, first year thick, and multi-year ice.							
ADR Requirements	Distinguish between ice free areas, first-year ice, and older ice.							
CDR Requirements	Distinguish between Ice free, new/fresh ice, nilas, grey white, first Year medium, first Year Thick, second year, and multiyear smooth and deformed ice.							

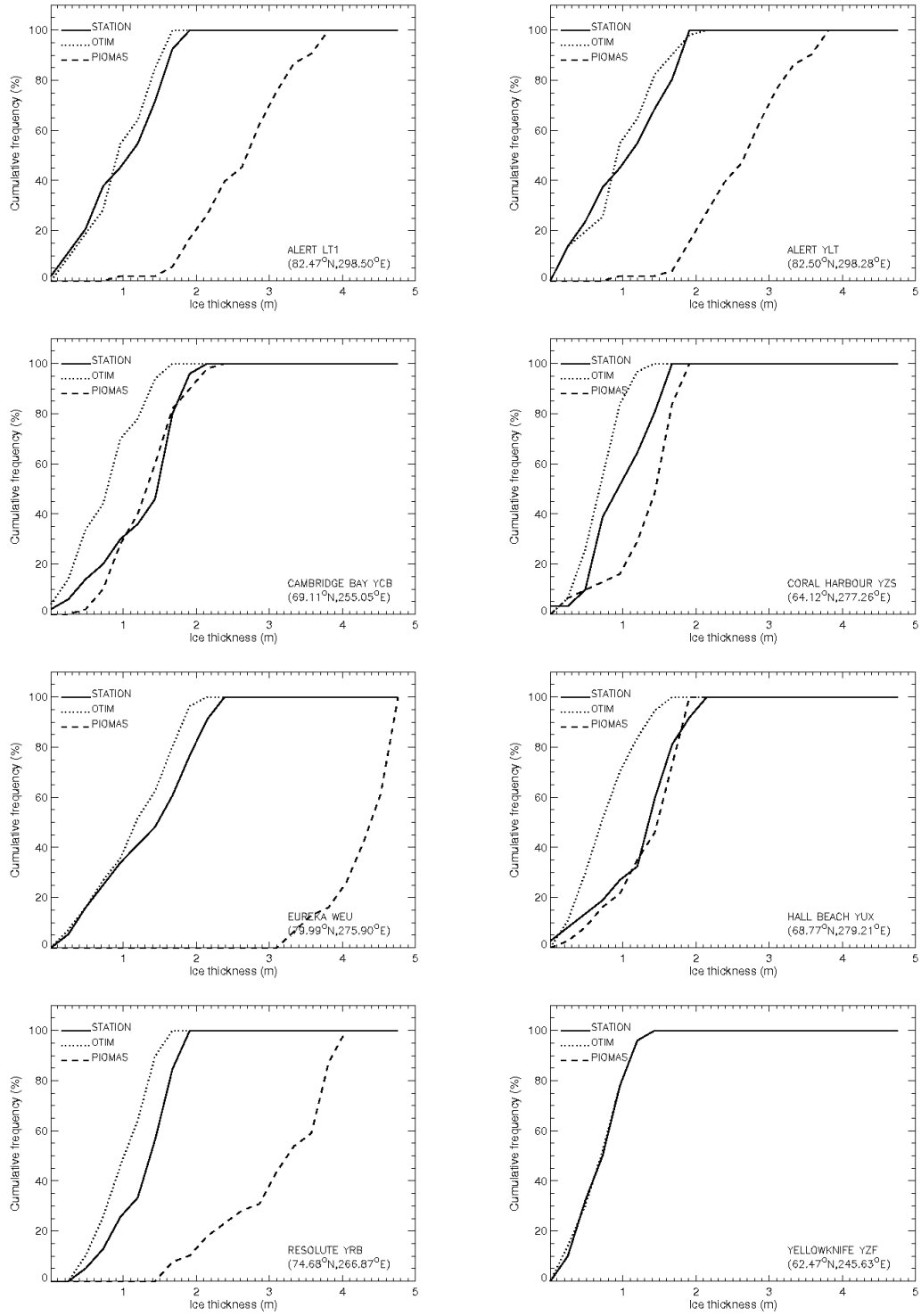

Figure 12. Comparisons of ice thickness cumulative distribution retrieved by OTIM with APP-x data, measured by stations, and simulated by the numerical model PIOMAS at the station locations shown in the lower-right corner of each plot.

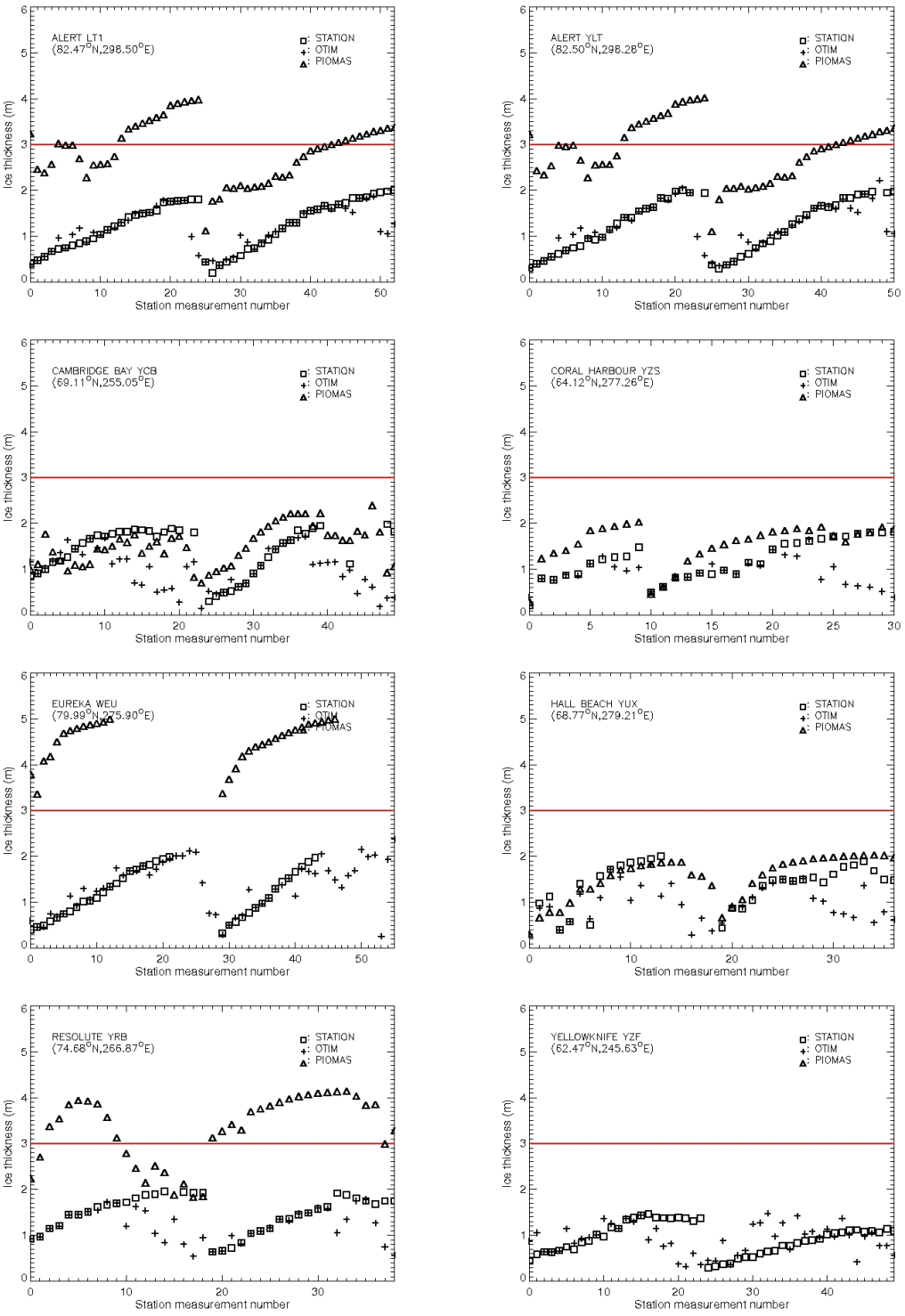

Figure 13. Comparisons of ice thickness values retrieved by OTIM with APP-x data, measured by stations, and simulated by the numerical model PIOMAS at the station locations shown in the lower-right corner of each plot.

4.2.1.4 Mooring Measurement Analysis

There are ice draft mooring data from the Beaufort Gyre Exploration Project (BGEP; http://www.whoi.edu/beaufortgyre/index.html) from 2003 up to the present at three mooring sites in the Beaufort Sea area. Since 2003, Upward Looking Sonars (ULS) were deployed beneath the Arctic ice pack on Beaufort Gyre Observing System (BGOS; http://www.whoi.edu/beaufortgyre) bottom-tethered moorings (Ostrom et al., 2004; Kemp et al., 2005). Over 15 million observations are acquired for every mooring location each year. Detailed ULS data processing can be found at http://www.whoi.edu/beaufortgyre/pdfs/BGOS%20ULS%20Data%20Processing%20Procedure.pdf. We used ice draft mooring data from 2003 and 2004 from three mooring sites because APP-x data are not available beyond 2004. The mooring ice draft is converted to ice thickness by multiplying a factor of 1.11 as was done for the submarine ice draft. The daily mean ice draft mooring data from 2003 to 2004 were used in the comparison, excluding the data from May through August due to the lack of retrievals of OTIM for the polar day period.

Table 11 lists mooring site location information, time period, and comparison statistical results. Figures 14 and 15 show the comparisons of the three data sets, i.e., OTIM using APP-x, PIOMAS simulations, and mooring measurements at three sites, as a cumulative frequency ice thickness distribution and as point-to-point comparisons. Table 11 provides the statistical results of ice thickness from OTIM and from mooring measurements for each of the three sites when both of them have valid ice thickness data. The overall error is comparable to the error of OTIM against submarine and station measurements.

Table 11. The OTIM validation results against mooring measurements over 2003-2004.

Mooring Location **OTIM**	**Thickness mean (m)**	**Bias mean (m)**	**Bias absolute mean (m)**
Site A (75°0.499'N, 149°58.660'W) OTIM	1.24 1.22	-0.02 (-1.2%)	0.19 (15.3%)
Site B (78°1.490'N, 149°49.203'W) OTIM	1.32 1.17	-0.15 (-11.4%)	0.29(21.9%)
Site C (76°59.232'N, 139°54.562'W) OTIM	1.32 1.20	-0.12 (-9.1%)	0.28 (21.2%)
ALL MOORING AVERAGE OTIM AVERAGE	1.29 1.20	-0.09 (-6.9%)	0.25 (19.4%)

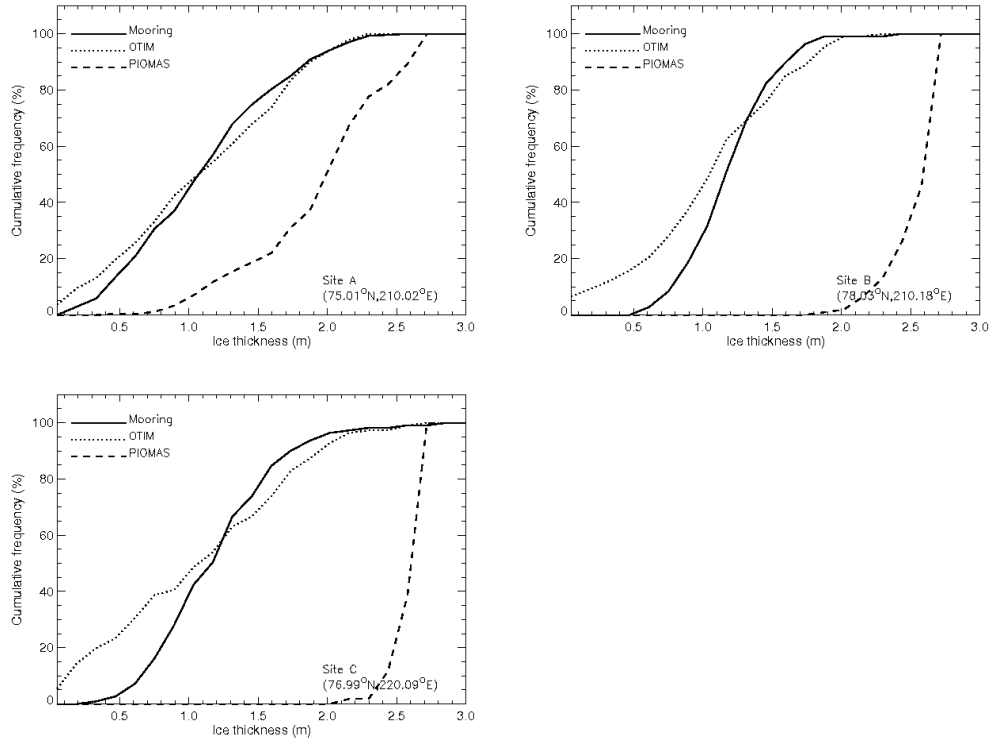

Figure 14. Comparisons of ice thickness cumulative distribution retrieved by OTIM with APP-x data, simulated ice thickness from the PIOMAS model and the ULS measurements at the mooring sites A, B, and C.

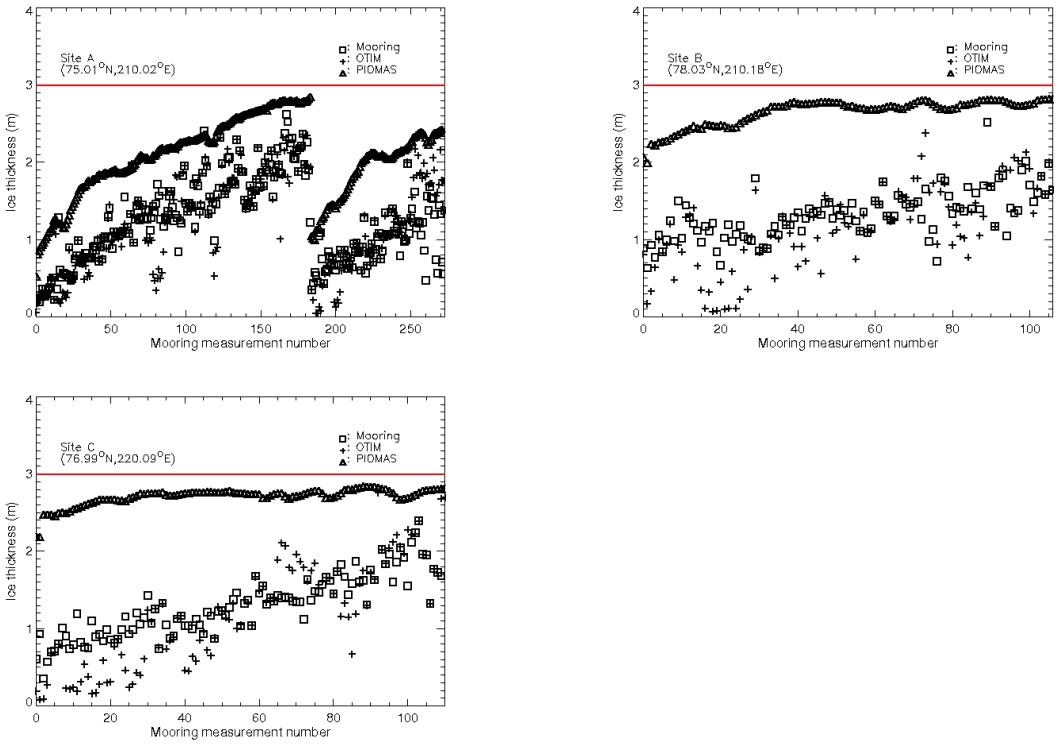

Figure 15. Comparisons of ice thickness values retrieved by OTIM with APP-x data, ULS measured ice thickness at mooring sites A, B, and C, and simulated ice thickness from the PIOMAS model.

4.2.1.5 Microwave Data Derived Ice Age Analysis

A data set of sea ice concentrations (the fraction, or percentage, of ocean area covered by sea ice) is available at http://nsidc.org/data/nsidc-0051.html. This data set is generated from brightness temperature data derived from the Nimbus-7 Scanning Multichannel Microwave Radiometer (SMMR) and Defense Meteorological Satellite Program (DMSP) -F8, -F11 and -F13 Special Sensor Microwave/Imager (SSM/I) radiances at a grid cell size of 25 x 25 km. These data include gridded daily (every other day for SMMR data) and monthly averaged sea ice concentrations for both the north and south polar regions. The data are generated using the NASA Team algorithm developed by the Oceans and Ice Branch, Laboratory for Hydrospheric Processes at NASA Goddard Space Flight Center (GSFC), and include data since 26 October 1978. The final data are produced from SMMR brightness temperature data processed at NASA GSFC and SSM/I brightness temperature data processed at the National Snow and Ice Data Center (NSIDC). These sea ice concentration data from passive microwave observations were used as an independent validation data resource for the ice age product. We used this microwave sea ice concentration data to derive sea ice age in the Arctic Ocean, i.e., ice free, first-year ice, and older ice by tracking daily sea ice concentration for each pixel over a year-long period. If an areal Sea Ice Concentration (SIC) is less than 15% all year round, it is identified as an ice free area; if it is less than 15% only for certain period of the year, it is identified as first-year ice area;

and if the areal SIC is never less than 15% on any day for a year, it is identified as an older ice area. In this way the ice age product derived from passive microwave data is reckoned as a proxy for ice age truth.

We collected 2412 data granules covering the Arctic from MODIS Terra and Aqua for March 2006, and applied our algorithm to derive the ice age product, and then composed all those MODIS granules to form a fully covered Arctic ice age map for comparison with the microwave derived ice age truth. Figure 16 shows the MODIS derived ice age (middle) with our algorithm from a composite of Terra & Aqua MODIS data in March 2006, and the ice age (left) derived from microwave ice concentration (NASA team algorithm) data using a tracking method over the year 2006. Inaccuracies in the MODIS cloud mask can severely affect the accuracy of ice thickness and age products. The performance of our ice age product algorithm is assessed by performance metrics of product accuracy and precision. The product accuracy is defined as the percentage ratio of the OTIM retrieval against truth, and the product precision is defined as the standard deviation of the errors between OTIM retrievals and truth. Tables 12, 13, and 14 list the statistical results between OTIM retrieval and truth in terms of total number of pixels in each category of ice free, first-year ice, and older ice, product accuracy, and product precision. As seen, overall our algorithm derived ice age product fulfills the requirements of an 80% product accuracy and a product precision of less than one age category. MODIS daytime data seem to have higher product accuracy and precision due to very few daytime data (small samples) available from MODIS Terra & Aqua for the Arctic Ocean in March 2006, and most of the Arctic Ocean is in the dark around the clock in the winter.

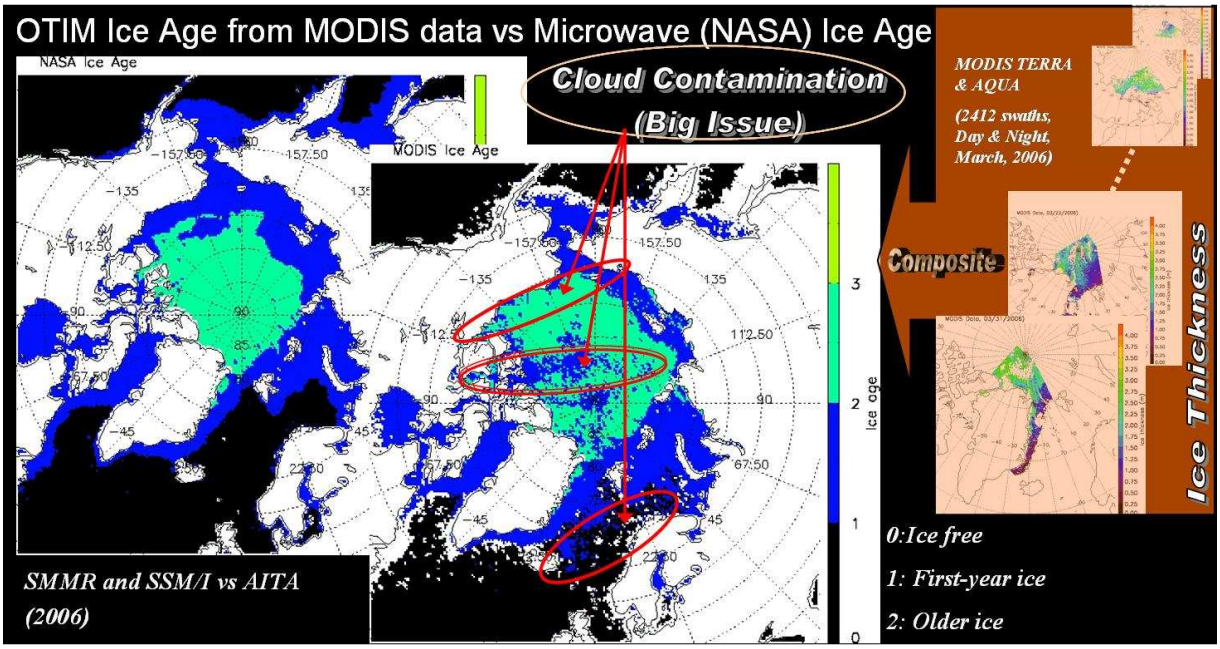

Figure 16. MODIS derived ice age (middle) using our algorithm from a composite of Terra & Aqua MODIS data in March 2006, and the ice age (left) derived from microwave ice concentration data (NASA team algorithm) using a tracking method over the year 2006.

Table 12. The statistical matrix of the comparison in ice age between OTIM derived ice age with MODIS data and NASA team algorithm derived ice age with passive microwave data.

Note: Number in each cell stands for the number of pixels that belong to the ice age categories corresponding to NASA and OTIM ice age classifications used to do statistics, i.e., accuracy and precision in ice age classification.		**NASA Ice Age Truth***			
		Ice Free	**First-year Ice**	**Older Ice**	**Total**
OTIM Ice Age This Study)	**Ice Free**	***(D&N:32278)*** ***(N:32288)*** ***(D:34681)***	***(D&N:0)*** ***(N:0)*** ***(D:0)***	***(D&N:0)*** ***(N:0)*** ***(D:0)***	**(D&N:32278)** **(N:32288)** **(D:34681)**
	First-year Ice	***(D&N:2381)*** ***(N:2371)*** ***(D:30)***	***(D&N:12623)*** ***(N:12615)*** ***(D:93)***	***(D&N:1141)*** ***(N:1141)*** ***(D:0)***	**(D&N:16145)** **(N:16127)** **(D:123)**
	Older Ice	***(D&N:52)*** ***(N:52)*** ***(D:0)***	***(D&N:2632)*** ***(N:2634)*** ***(D:0)***	***(D&N:5919)*** ***(N:5919)*** ***(D:0)***	**(D&N:8603)** **(N:8605)** **(D:0)**
	Total	**(D&N:34711)** **(N:34711)** **(D:34711)**	**(D&N:15255)** **(N:15249)** **(D:93)**	**(D&N:7060)** **(N:7060)** **(D:0)**	**(D&N:57026)** **(N:57020)** **(D:34804)**

***** D=Day, N=Night, D&N=Day and Night

Table 13. The statistical results in terms of product accuracy for the comparison in ice age between OTIM derived ice age with MODIS data and the NASA team algorithm derived ice age with passive microwave data.

Ice Age (OTIM vs Microwave)*	
Statistics	**Accuracy**[!]
Ice Free	D&N:93%, N:93%, D:~100%
First-year Ice	D&N:92%, N:92%, D:~100%
Older Ice	D&N:84%, N:84%, D:~100%
All	D&N:89%, N:89%, D:~100%
Error Sources	1. *Ice identification algorithm* 2. *Cloud mask/shadow detection* 3. *Relationship between thickness and age* 4. *Ice motion/Dynamic processes*

* D=Day, N=Night, D&N=Day and Night

Table 14. The statistical results in terms of product precision for the comparison in ice age between OTIM derived ice age with MODIS data and NASA team algorithm derived ice age with passive microwave data.

Note: Number in each cell stands for the number of pixels that belong to the ice age category difference corresponding to NASA and OTIM ice age classifications used to do statistics, i.e., accuracy and precision in ice age classification.	**Ice Age Difference (OTIM vs Microwave)**		
	No Difference	**1 Category Difference**	**2 Category Difference**
	(D&N:49820) (N:49822) (D:34774)	(D&N:7154) (N:7146) (D:30)	(D&N:52) (N:52) (D:0)
Precision	**(D&N:0.34 Category)** **(N:0.34 Category)** **(D:0.03 Category)**		

* D=Day, N=Night, D&N=Day and Night

4.2.2 Error Budget

In estimating ice thickness using the OTIM, many factors affect the accuracy of ice thickness. The uncertainties from all of the input controlling variables in the OTIM will propagate into ice thickness through the parameterizations and model algorithms. Theoretically and mathematically speaking, we can describe the ice thickness estimate as a function of heat fluxes and surface albedo and transmittance:

$$\hat{h}_i = f(\hat{\alpha}_s, \hat{i}_0, \hat{F}_r, \hat{F}_l^{up}, \hat{F}_l^{dn}, \hat{F}_s, \hat{F}_e, \hat{F}_c, \hat{F}_a) \qquad (31)$$

where the variables with carets "^" are the variables defined in Equation (1). In the OTIM model we used parameterization schemes (Key et al., 1996) as described in previous sections to calculate $\hat{F}_l^{up}, \hat{F}_l^{dn}, \hat{F}_s, \hat{F}_e, \hat{F}_c$, all of which are functions of surface skin and air temperatures ($\boldsymbol{T_s}$, $\boldsymbol{T_a}$), surface air pressure (P_a), surface air relative humidity (R), ice temperature (T_i), wind speed (U), cloud amount (C), and snow depth (h_s); therefore, ice thickness is actually the function of those variables expressed in Equation (32):

$$\hat{h}_i = f(\hat{\alpha}_s, \hat{i}_0, \hat{F}_r, \hat{T}_s, \hat{T}_i, \hat{T}_a, \hat{P}_a, \hat{R}, \hat{U}, \hat{C}, \hat{h}_s, \hat{F}_a) \qquad (32).$$

Suppose the true ice thickness h_i is estimated from the true values of all controlling variables in Equation (32), and let x_i represent the variables in equation (32) with true values, and $\hat{x}_i$

represent those variable with estimated values, and *x's* subscript *i* is between 1 and 12 representing the 12 variables in Equation (32); thus, if the uncertainties in the controlling variables are independent and random, the statistics of the error $(\hat{h}_i - h_i)$ can be expressed in terms of the uncertainties in the variables on which it depends:

$$(\hat{h}_i - h_i) = \sum (\hat{x}_i - x_i) \frac{\partial h_i}{\partial x_i} \qquad (33)$$

or the variance in the thickness error, as

$$\sigma_{h_i}^2 = \sum \sigma_{x_i}^2 (\frac{\partial h_i}{\partial x_i})^2 \qquad (34).$$

However, as discussed by Key et al. (1997), if the variables are not independent of each other, then the covariances between them must be considered. Unfortunately, data needed to estimate the covariance between all pairs of variables are often not available. If the covariance between pairs of variables is unknown, then it can be shown (Taylor, 1982) that the total uncertainty will never exceed

$$\sigma_{h_i} \le \sum \sigma_{x_i} | \frac{\partial h_i}{\partial x_i} | \qquad (35)$$

Tables 15 and 16 give estimates of the partial derivatives needed in Equations (33), (34), and (35), computed using differences ($\Delta h_i/\Delta x_i$). These partial derivatives can be used for calculating the sensitivity of the ice thickness to errors in the controlling variables.

The estimated uncertainties in the controlling variables in Equation (32), e.g. surface skin temperature T_s, are now used to assess the accuracy with which ice thickness can be estimated using satellite data products. Since ice thickness varies nonlinearly with respect to the controlling variables under investigation, its sensitivity to errors varies over the range of the input controlling variables. Therefore, uncertainty in ice thickness is estimated for a set of reference values that represent the typical values for certain thick ice as listed in Tables 15 and 16.

To estimate σ_{h_i}, we first need to estimate the uncertainties of all controlling variables in Equation (32). According to Wang and Key (2005), for the satellite retrieved surface broadband albedo α_s, the uncertainty would be as large as 0.10 in absolute magnitude. Regarding the ice slab transmittance i_0, we use an absolute uncertainty of 0.05 in this study, which is in part arbitrary and likely larger than the actual value. The satellite retrieved surface downward shortwave radiation flux F_r can be biased high or low by 20% of the actual value or 35 W m^{-2} as compared with in-situ measurements (Wang and Key, 2005). Wang and Key (2005) also estimated the uncertainties in satellite-derived surface skin temperature T_s and cloud amount C with respect to the Surface Heat Balance of the Arctic Ocean (SHEBA) ship measurements (Maslanik et al., 2001) that can be as large as 2 K and 0.25 in absolute magnitude, respectively; we use 2 K as the surface air temperature T_a uncertainty as well. Since the surface may be covered with a layer of

snow, ice slab temperature T_i may be different from T_s, therefore assuming $T_i = T_s$ may introduce additional error in the ice thickness estimation; we elect to assign 5 K uncertainty in T_i to estimate its impact on the ice thickness since there is no known information about the difference between T_i and T_s, and the satellite can only retrieve surface skin temperature T_s, not T_i. The uncertainties in surface air pressure and relative humidity together with surface temperature will affect the ice thickness estimation indirectly through the impact of turbulent sensible and latent heat fluxes. As a change of 50 *hPa* in surface air pressure may induce changing weather patterns, we take 50 *hPa* as maximum possible uncertainty of surface air pressure. The uncertainty in geostrophic wind U_G could be 2 m s^{-1} as determined by the buoy pressure field (Thorndike and Colony, 1982), and the relationship $U = 0.34U_G$ gives the uncertainty in surface wind speed U of 0.7 m s^{-1}, we take 1 m s^{-1} as possible uncertainty in this study. An uncertainty of 10% in surface air relative humidity is adopted in this work. Snow cover directly affects conductive heat flux, surface albedo, and the radiative fluxes at the interface of the ice and snow. Snow depth h_s plays a big role, however, accurate and spatially wide covering measurements are usually not available coincidentally in time and space with satellite observations, and also depth changes over time with wind and topography. It is hard to know the uncertainty in snow depth estimation, however, we think it is reasonable to give 50% of the given snow depth as its uncertainty in general. The last uncertainty source is the surface residual heat flux F_a, which is associated with ice growth, ablation, and possible horizontal heat gain/loss. In the case of no melting and horizontal heat gain/loss, F_a is zero, which is widely accepted by ice models if the surface temperature is below the freezing point. We set the uncertainty of F_a at 2 W m^{-2} as an initial guess. The overall error caused by the uncertainties in those controlling variables for ice thickness estimation may not be equal to the summation of all errors from each individual uncertainty source because the opposite effects may cancel each other among the uncertainty sources resulting in fewer errors as mathematically described by Equation (35).

Tables 15 and 16 list the controlling variables used in the ice thickness sensitivity study for daytime and nighttime cases with the aforementioned uncertainties in controlling variables and their impacts for a typical ice thickness of 1 meter. The results of this sensitivity study are shown graphically in Figures 17 and 18 based on the reference ice thickness values of 0.3, 1.0, 1.8 meters with those expected uncertainties in controlling variables. The bars give the overall range in the ice thickness corresponding to the uncertainties listed in the Tables. Plus signs in Figures 17 and 18 are the ice thickness values for positive uncertainties in the indicated variables; minus signs show the direction of change in ice thickness for a decrease in the controlling variable value.

Table 15. Sensitivity of ice thickness estimates to uncertainties in the controlling variables during a daytime case with a reference ice thickness of 1 meter.

Name	***Ref. Value***	***Error (Dx)***		***IceThk_Dh***		***IceThk_Dh/h***		***IceThk_Dh/Dx***	
T_s (K)	253.23	+2.000	-2.000	-0.235	+0.245	-0.235	+0.245	-0.117	-0.122
T_i (K)	253.23	+5.000	-5.000	-0.008	+0.008	-0.008	+0.008	-0.002	-0.002
h_s (m)	0.20	+0.100	-0.100	-0.654	+0.654	-0.654	+0.654	-6.544	-6.544
R (%)	90.00	+9.000	-9.000	+0.024	-0.024	+0.024	-0.024	+0.003	+0.003
U (m/s)	5.00	+1.000	-1.000	+0.316	-0.208	+0.316	-0.208	+0.316	+0.208
P_a (hPa)	1000.00	+50.00	-50.00	+0.066	-0.063	+0.066	-0.063	+0.001	+0.001
α_s (0~1)	0.85	+0.100	-0.100	-0.757	+2.195	-0.757	+2.195	-7.566	-21.953

T_r (0~1)	0.05	+0.050	-0.050	-0.086	+0.092	-0.086	+0.092	-1.711	-1.848
F_r (w/m^2)	101.44	+20.288	-20.288	+0.395	-0.295	+0.395	-0.295	+0.019	+0.015
F_a (w/m^2)	0.00	+2.000	-2.000	-0.212	+0.260	-0.212	+0.260	-0.106	+0.130
C (0~1)	0.50	+0.250	-0.250	+0.297	-0.639	+0.297	-0.639	+1.189	+2.555

Table 16. Sensitivity of ice thickness estimates to uncertainties in the controlling variables during a nighttime case with a reference ice thickness of 1 meter.

Name	*Ref. Value*	*Error (Dx)*		*IceThk_Dh*		*IceThk_Dh/h*		*IceThk_Dh/Dx*	
T_s (K)	241.09	+2.000	-2.000	-0.172	+0.179	-0.172	+0.179	-0.086	-0.090
T_i (K)	241.09	+5.000	-5.000	-0.008	+0.008	-0.008	+0.008	-0.002	-0.002
h_s (m)	0.20	+0.100	-0.100	-0.667	+0.667	-0.667	+0.667	-6.666	-6.666
R (%)	90.00	+9.000	-9.000	+0.006	-0.006	+0.006	-0.006	+0.001	+0.001
U (m/s)	5.00	+1.000	-1.000	+0.166	-0.133	+0.166	-0.133	+0.166	+0.133
P_a (hPa)	1000.00	+50.00	-50.00	+0.043	-0.041	+0.043	-0.041	+0.001	+0.001
F_a (w/m^2)	0.00	+2.000	-2.000	-0.137	+0.155	-0.137	+0.155	-0.068	0.078
C (0~1)	0.50	+0.250	-0.250	+0.248	-0.476	+0.248	-0.476	+0.992	+1.903

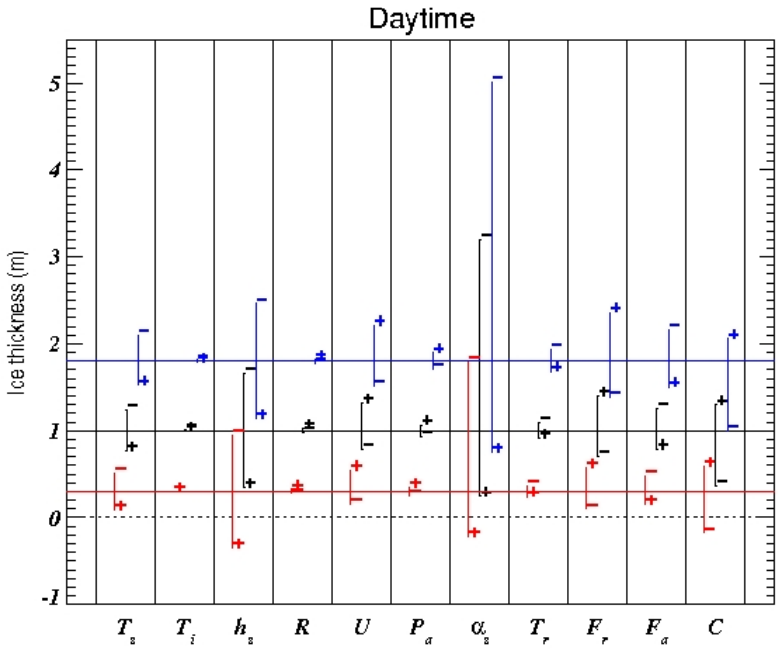

Figure 17. Sensitivity of ice thickness to expected uncertainties in the controlling variables for a daytime case with a reference ice thickness of 0.3 (red), 1 (black), and 1.8 (blue) meters.

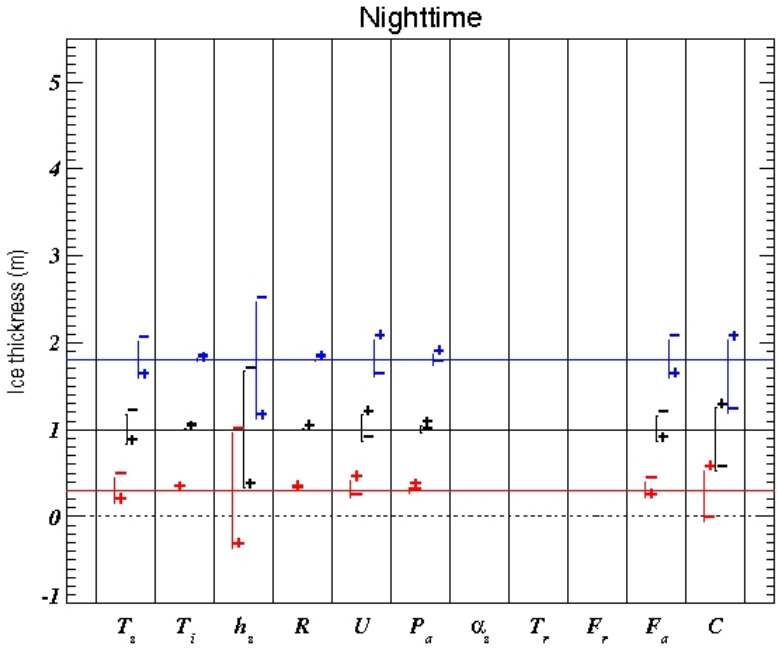

Figure 18. Sensitivity of ice thickness to expected uncertainties in the controlling variables for a nighttime case with a reference ice thickness of 0.3 (red), 1 (black), and 1.8 (blue) meters.

5 Practical Considerations

5.1 Numerical Computation Considerations

The AITA is implemented sequentially. Because the ice thickness retrieval via OTIM relies on the values of the ancillary data flags, the ancillary data flags need to be computed first. The AITA will be implemented into the AIT and uses its numerical routines for processing.

5.2 Programming and Procedural Considerations

The AITA requires knowledge of spatial information for accurate pixel geographic locations and land mask information for identifying sea, lake, river, etc. In addition, the temporal information is required for each pixel regarding the solar radiation in case the daytime algorithm is used. Beyond these requirements, the AITA is purely a pixel by pixel algorithm.

5.3 Quality Assessment and Diagnostics

The following procedures are recommended for diagnosing the performance of the AITA.

- Monitor the percentage of pixels retrieved for ice thickness, and check the value uniformity over the small and smooth areas without cracks, melting ponds, and leads.
- Check ancillary input data such as surface skin temperature, air temperature, humidity, wind speed, and snow depth for all pixels of the AITA. See how changes in those ancillary variables affect the ice thickness estimation.
- Periodically image the individual test results to look for artifacts or non-physical behaviors.
- Maintain a close collaboration with the other teams using the AITA in their product generation.

5.4 Exception Handling

The AITA includes checking the validity of input data before applying the OTIM and ice age algorithm. The AITA also expects the main processing system (i.e., AIT) to flag any pixels with missing geolocation or viewing geometry information.

The AITA does check for conditions where the AITA can not be performed. These conditions include missing input variables values and unsolvable numerical solutions. In these cases, the appropriate flag is set to indicate that no ice thickness and age are produced for that pixel.

5.5 Algorithm Validation

As discussed and detailed in section 4.2, the validations were performed with modeled ice thickness data from PIOMAS, submarine and mooring site measurements, and in-situ station measurements. Our testing and validations span multiple years for every season, and cover both sea ice and lake ice, though most of them are within the Arctic Ocean where the submarine, mooring sites, and station measurements were made for years.

The mean absolute error is 0.31 m for samples with a mean ice thickness of 1.80 m, i.e., a 17% mean absolute bias when comparing to the submarine uplooking sonar ice draft measurements in terms of ice thickness. The results of comparisons with mooring sites and in-situ Canadian station measurements are similar. In terms of ice age classifications, the algorithm can easily meet the MRD requirements by classifying ice into ice-free, first-year, and older ice with an accuracy greater than 80% and a product precision of less than one age category.

6 Assumptions and Limitations

The following sections describe the current limitations and assumptions in the current version of the AITA.

6.1 Performance

The following list contains the current assumptions and proposed mitigation strategies.

1. Atmospheric profile and wind speed data are available from NWP or other teams' retrieved products. In case no profile data are available, it is a valid assumption as used by other researchers that the surface air temperature generally is about 0.5 ~ 2 degree higher than the ice/snow surface temperature depending on the cloud conditions, and the relative humidity is about 90% over ice/snow, and a wind speed of 6~10 m/s at night. But wind speed should be observed or simulated to guarantee it is realistic.

2. Radiation fluxes are available from NWP or other teams' products, otherwise parameterizations will be used and assumed reliable and accurate enough for each pixel. (*Use parameterization schemes over ice and/or snow surface from Bennett (1982), Ohmura (1981), Jacob (1978) as recommended*).

3. Snow maps and climatological depths are available from NWP or other teams' products, or a general assumption of 2~50 cm snow depth will be used over ice. (*Use snow information from NWP or elsewhere*).

4. Land mask maps are available to identify different surface types.

5. All of the static ancillary data are available at the pixel level. (*Reduce the spatial resolution of the surface type, land mask and/or coast mask to pixel size*).

6.2 Assumed Sensor Performance

We assume the sensors will meet its current specifications and retrieved products from other teams will be accurate enough for the AITA, otherwise AITA built-in parameterization schemes will be used for certain input variables. The AITA will be critically dependent on the following retrieved products.

- Surface skin and air temperature.
- Surface broadband albedo
- Radiation fluxes at the surface.
- Snow depth.

- Atmospheric moisture and wind.

6.3 Pre-Planned Product Improvements

The AITA serves other applications. Its development is closely tied to the development and feedback from the other team algorithms. At this point, it is therefore difficult to predict what the future modifications will be. However, the following discussion contains our current best guess of the future AITA modifications.

6.3.1 Daytime Algorithm Modification

Solar radiation is inevitably involved in the daytime ice thickness retrieval, making the OTIM extremely difficult to solve analytically for ice thickness due to the complicated ice/snow micro-macro physical properties in the solar spectrum, which vary significantly with changes in ice/snow clarity, density, chemicals contained, salinity, particle size and shape, structure, and thickness itself that are hard to know beforehand. We plan to search and/or develop reliable and efficient parameterizations for ice/snow reflectance, transmittance, emissivity, conductivity, and others as well as to develop a parameterization scheme for estimating residual heat flux for taking into account the un-equilibrium state at the interface between ice/snow and the atmosphere, in particular, for daytime conditions.

6.3.2 Optimization

The OTIM has been optimized to minimize computation time. Other ways to optimize product generation will continue to be investigated.

7 References

Andreas, E.L. and S.F. Ackley, 1982, On the differences in ablation seasons of Arctic and Antarctic sea ice, *J. Atmos. Sci.*, 39, 440-447.

Bennett, T.J., 1982, A coupled atmosphere-sea ice model study of the role of sea ice in climatic predictability, *J. Atmos. Sci.*, 39, 1456-1465.

ABDERRAHIM BENTAMY, KRISTINA B. KATSAROS, ALBERTO M. MESTAS-NUN˜ EZ, WILLIAM M. DRENNAN, EVAN B. FORDE,1 AND HERVE´ ROQUET, 2003, Satellite Estimates of Wind Speed and Latent Heat Flux over the Global Oceans, *J. Climate*, Vol.16, 637-656, 2003.

Berliand, T. C., 1960: Method of climatological estimation of global radiation. *Meteor. Gidrol.*, 6, 9-12.

Burt, W.V., 1954, Albedo over wind roughened water, *Journal of Meteorology*, 11, 283-290.

Chernigovskiy, N.T., 1963, Radiation properties of the central Arctic ice cover, Trudy Arkticheskogo I Antarkticheskogo Nauchno-Issledovatel'skogo Instituta, Tom 253, 249-260.

Cox, G.F.N. and W.F. Weeks, 1974, Salinity variations in sea ice, *J. Glaciol.*, 13, 109-120.

Curry, A. Judith and Peter J. Webster, 1999, <<Thermodynamics of Atmospheres & Oceans>>, pp.277, ISBN 0-12-199570-4, Academic Press.

Doronin, Y.P., 1971, Thermal Interaction of the Atmosphere and Hydrosphere in the Arctic, P.85, *Israel Program for Sci. Trans.*, Jerusalem, 1971.

Ebert, E. and J.A. Curry, 1993: An intermediate one-dimensional thermodynamic sea ice model for investigating ice-atmosphere interactions. *J. Geophys. Res.*, 98, 10085-10109.

Efimove, N.A., 1961, On methods of calculating monthly values of net longwave radiation, *Meteorol. Gidrol.*, 10, 28-33.

Fowler, C., J. Maslanik, T. Haran, T. Scambos, J. Key, and W. Emery. 2002. AVHRR Polar Pathfinder twice-daily 25 km EASE-Grid composites. Boulder, CO: National Snow and Ice Data Center. *Digital media*.

Fowler, C., J. Emery, and J. Maslanik, 2004, Satellite-Derived Evolution of Arctic Sea Ice Age: October 1978 to March 2003, IEEE GEOSCIENCE AND REMOTE SENSING LETTERS, VOL. 1, NO. 2, 71-74, APRIL 2004.

Grenfell, T. C. and G. A. Maykut, 1977, The optical properties of ice and snow in the Arctic Basin, *J. Glaciol.*, 18, 445-63.

Grenfell, T. C., 1979, The effects of ice thickness on the exchange of solar radiation over the polar oceans, *J. Glaciol.*, 22, 305-20.

Grenfell, T.C. and D.K. Perovich, 1984, Spectral albedos of sea ice and incident solar irradiance in the southern Beaufort Sea, *Journal of Geophysical Research*, Vol.89, C7, p. 3573-3580.

Grenfell, T.C. and D.K. Perovich, 2004, Seasonal and spatial evolution of albedo in a snow-ice-land-ocean environment, *J. Geophy. Res.*, 109, No. C1.

Jacobs, J.D., 1978: Radiation climate of Broughton Island. In: R. G. Barry and J. D. Jacobs, Energy budget studies in relation to fast-ice breakup processes in Davis Strait, Occas. Pap. 26,105-120. Inst. of Arctic and Alp. Res., Univ. of Colorado, Boulder, CO.

Jin, Z., K. Stamnes, and W.F. Weeks, 1994, The effect of sea ice on the solar energy budget in the atmosphere-sea ice-ocean system: A model Study, *J. Geophys. Res.*, 99, No. C12, 25,281-25,294.

Kara, A.B., P.A. Rochford, and H.E. Hurlburt, 2000, Efficient and Accurate Bulk Parameterizations of Air–Sea Fluxes for Use in General Circulation Models, *J. of Atmosph. and Oceanic Tech.*, Vol.17, 1421-1438, 2003.

Kemp, J., K. Newhall, W. Ostrom, R. Krishfield, and A. Proshutinsky (2005), The Beaufort Gyre Observing System 2004: Mooring Recovery and Deployment Operations in Pack Ice, Technical Report of the Woods Hole Oceanographic Institution, WHOI-2005-05, 33pp.

Key, 2002, The Cloud and Surface Parameter Retrieval (CASPR) System for Polar AVHRR, NOAA/NESDIS/STAR, Madison, WI, available online at the http://stratus.ssec.wisc.edu.

Key, J.R., R.A. Silcox, and R.S. Stone, 1996, Evaluation of surface radiative flux parameterizations for use in sea ice models, *J. Geophys. Res.*, Vol.101, No. C2, 3839-3849.

Key, J.R., A.J. Schweiger, and R.S. Stone, 1997, Expected uncertainty in satellite-derived estimates of the surface radiation budget at high latitudes, *J. Geophys. Res.*, Vol.102, No. C7, 15,837-15,847.

Kovacs, A., 1996. Sea ice: Part I. Bulk salinity versus ice floe thickness. US Army Cold Regions Research and Engineering Laboratory, CRREL Report 96-7.

Laevastu, T., 1960, Factors affecting the temperature of the surface layer of the sea, *Comments Phys. Math.*, 25, 1.

Langleben, M.P., 1971, Albedo of melting sea ice in the southern Beaufort Sea, *Journal of Glaciology*, 10, 101-104.

Lindsay, R.W., 1998, Temporal Variability of the Energy Balance of Thick Arctic Pack Ice, *J. Climate*, Vol.11, 313-333, March 1998.

Maslanik, J. A., J. R. Key, C. W. Fowler, T. Nguyen, and X.Wang, 2001: Spatial and temporal variability of satellite-derived cloud and surface characteristics during FIRE-ACE. *J. Geophys. Res.*, 106 (D14), 15 233–15 249.

Maslanik, J.A., C. Fowler, J. Stroeve, S. Drobot, J. Zwally, D. Yi, and W. Emery, 2007, A younger, thinner Arctic ice cover: Increased potential for rapid, extensive sea-ice loss, *Geophys. Res. Lett.*, 34, L24501, doi:10.1029/2007GL032043.

Maykut, G.A., and N. Untersteuner, 1971, Some results from a time-dependent thermodynamic model of sea ice, *J.G.R.*, Vol. 76, pp.1550-1575.

Maykut, G.A. and P.E. Church, 1973, Radiation climate of Barrow, Alaska, 1962-66, *J. Appl. Meteorol.*, 12, 620-628.

Moritz, R.E., 1978. A model for estimating global solar radiation, Energy budget studies in relation to fast-ice breakup processes in Davis Strait, edited by R.G. Barry and J.D. Jacobs, Occas.l Pap. 26pp. 121-142, Inst. Of Arctic and Alp. Res., Univ. of Colo., Boulder.

National Snow and Ice Data Center. 1998, updated 2006. Submarine upward looking sonar ice draft profile data and statistics. Boulder, CO: National Snow and Ice Data Center/World Data Center for Glaciology. *Digital media*.

Ohmura, A., 1981, Climate and energy balance of the Arctic tundra, Zürcher Geogr. Schr. 3, 448 pp., Geogr. Inst., Zürich, Switzerland.

Ostrom, W., J. Kemp, R. Krishfield, and A. Proshutinsky (2004), Beaufort Gyre Freshwater Experiment: Deployment Operations and Technology in 2003, Technical Report of the Woods Hole Oceanographic Institution, WHOI-2004-01, 32 pp.

Perovich, D.K., 1996, The Optical Properties of Sea Ice, *CRREL Monograph, 96-1*. 25 pp., May.

Persson, P. O. G., C. W. Fairall, E. L. Andreas, P. S. Guest, and D. K. Perovich (2002), Measurements near the Atmospheric Surface Flux Group tower at SHEBA: Near-surface conditions and surface energy budget, *J. Geophys. Res.*, 107(C10), 8045, doi:10.1029/2000JC000705.

Rees, W.G., 1993, Infrared emissivities of Arctic land cover types, *Int. J. Remote Sensing*, 14, 1013-1017.

Schmetz, P.J. and E. Raschke, 1986, Estimation of daytime downward longwave radiation at the surface from satellite and grid point data, *Theor. Appl. Climatol.*, 37, 136-149.

Schrodere, D., T. Vihma, A. Kerber and B. Brummer, 2003, On the parameterization of turbulent surface fluxes over heterogeneous sea ice surfaces, *J. Geophys. Res.*, 108 (C6), doi:10.1029/2002JC001385.

Shine, K.P., 1984, Parameterization of shortwave flux over high albedo surfaces as a function of cloud thickness and surface albedo, *Q. J. R. Meteorol. Soc.*, 110, 747-764.

Shine, K.P. and A. Henderson-Sellers, 1985, The sensitivity of a thermodynamic sea ice model to changes in surface albedo parameterization, *J. Geophys. Res.*, 90, 2243-2250.

Taylor, J.R., An Introduction to Error Analysis, 270 pp., Univ. Sci. Books, Mill Valley, Calif., 1982.

Thorndike, A. S., D. A. Rothrock, G. A. Maykut, and R. Colony, 1975: The thickness distribution of sea ice, *J. Geophys. Res.*, 80, 4501-4513.

Tucker, W.B., III, J.W.Weatherly, D.T. Eppler, L.D. Farmer, and D.L. Bentley, 2001, Evidence for rapid thinning of sea ice in the western Arctic Ocean at the end of the 1980s, *Geophys. Res. Lett.*, 28(14), 2851-2854.

Tuomo M. Saloranta, 2000, Modeling the evolution of snow, snow ice and ice in the Baltic Sea, *Tellus*, 52A, 93-108.

Thornedike, A.S., D.A. Rothrock, G.A. Maykut, and R.Colony, 1975, The thickness distribution of sea ice, *J. Geophys. Res.*, 80, 4501-4513.

Untersteiner, N., 1964, Calculations of temperature regime and heat budget of sea ice in the central Arctic, *J. Geophys. Res.*, 69, 4655-4766.

Wang, X. and J. Key, 2003, Recent trends in Arctic surface, cloud, and radiation properties from space, *Science*, 299(5613), 1725-1728.

Wang, X., J. Key, and Y. Liu, 2010, A thermodynamic model for estimating sea and lake ice thickness with optical satellite data, *J. Geophys. Res.*, revision submitted, Sept. 2010.

Yen, Y.-C., 1981: Review of thermal properties of snow, ice and sea ice. CRREL Rep. 81-10, 27 pp. [*Available from Cold Regions Research and Engineering Laboratory, 72 Lyme Rd., Hanover, NH 03755.*]

Yu, Y. and D.A. Rothrock, 1996, Thin ice thickness from satellite thermal imagery, *J. Geophys. Res.*, Vol.101, No. C10, 25,753-25,766.

Yu, Y., G.A. Maykut, and D.A. Rothrock, 2004, Changes in the thickness distribution of Arctic sea ice between 1958-1970 and 1993-1997, *J. Geophys. Res.*, 109, C08004, doi:10.1029/2003JC001982.

Zhang, J., and D.A. Rothrock, 2003, Modeling global sea ice with a thickness and enthalpy distribution model in generalized curvilinear coordinates, *Mon. Wea. Rev.*, 131(5), 681-697.

Zhang, J., and D.A. Rothrock, 2001, A thickness and enthalpy distribution sea-ice model, *J. Phys. Oceanogr.*, 31, 2986-33001.

Zillman, J.W., 1972, A study of some aspects of the radiation and heat budgets of the southern hemisphere oceans, Meteorol. Stud. Rep. 26, Bur. Of Meteorol., Dep. Of the Inter., Canberra, A.C.T.

Appendix A. Conductive heat flux for two-layer system with snow over ice

Consider a two-layer system, with a slab of ice covered by a layer of snow as shown below. We assume the temperature gradients in the snow and ice are each linear and thus conductive heat

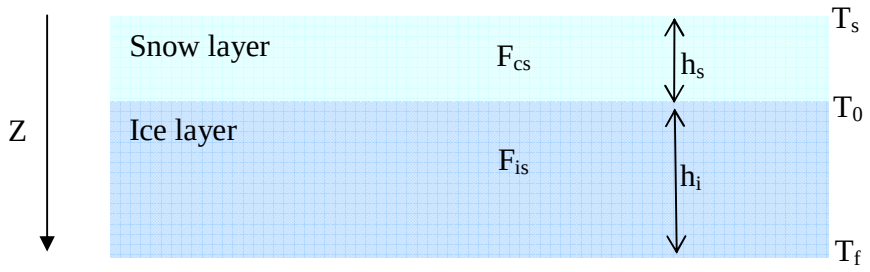

flux is constant with depth. At the snow/ice interface, the conductive flux in the snow must equal the conductive flux in the ice, i.e., $F_{ci} = F_{cs}$. As we define the direction to the snow/ice is positive, so we can derive the conductive heat flux for the two-layer system with a snow layer covering a slab of ice as shown below. The downward direction is defined as positive, so $F_c=k\cdot dT/dh$, where dT is temperature difference, and dh is the snow/ice thickness.

$$F_c = k\frac{dT}{dZ}, \text{and so for the snow layer, we have } F_{cs} = k_s\frac{T_0 - T_s}{h_s}, \text{and the same for the ice slab,}$$

$$F_{ci} = k_s\frac{T_f - T_0}{h_i}, \text{ so we have } k_s\frac{T_f - T_0}{h_i} = k_s\frac{T_0 - T_s}{h_s}, \text{after series of derivation, we finally get}$$

$$T_0 = \frac{k_s h_i T_s + k_i h_s T_f}{k_i h_s + k_s h_i}, \text{ therefore } F_{cs} = \frac{k_i k_s}{k_i h_s + k_s h_i}(T_f - T_s), F_c = F_{cs} = \frac{k_i k_s}{k_i h_s + k_s h_i}(T_f - T_s).$$